Accepted Manuscript

Discover 4β-*NH*-(6-aminoindole)-4-desoxy-podophyllotoxin with nanomolar-potency antitumor activity by improving the tubulin binding affinity on the basis of a potential binding site nearby colchicine domain

Wei Zhao, Long He, Tian-Le Xiang, Ya-Jie Tang

Please cite this article as: W. Zhao, L. He, T.-L. Xiang, Y.-J. Tang, Discover 4β-*NH*-(6-aminoindole)-4-desoxy-podophyllotoxin with nanomolar-potency antitumor activity by improving the tubulin binding affinity on the basis of a potential binding site nearby colchicine domain, *European Journal of Medicinal Chemistry* (2019), doi: https://doi.org/10.1016/j.ejmech.2019.03.006.

Discover 4β-*NH*-(6-aminoindole)-4-desoxy-podophyllotoxin with nanomolar-potency antitumor activity by improving the tubulin binding affinity on the basis of a potential binding site nearby colchicine domain

Wei Zhao [a, 1], Long He [b, 1], Tian-Le Xiang [c] and Ya-Jie Tang [a, b, *]

[a] *State Key Laboratory of Microbial Technology, Shandong University, Qingdao 266237, China*

[b] *Hubei Key Laboratory of Industrial Microbiology, Hubei Provincial Cooperative Innovation Center of Industrial Fermentation, Key Laboratory of Fermentation Engineering (Ministry of Education), Hubei University of Technology, Wuhan 430068 China*

[c] *No.11 Middle School of Wuhan, Wuhan 430068 China*

*Corresponding author. Tel. & Fax: +86-27-5975.0491 Email: yajietang@sdu.edu.cn

[1] These authors contributed equally to this work

CONFLICT OF INTEREST: No potential conflicts of interest were disclosed.

Graphical Abstract

A potential binding site nearby colchicine domain

Micromolar-potency   Nanomolar-potency

Discover 4β-*NH*-(6-aminoindole)-4-desoxy-podophyllotoxin with nanomolar-potency antitumor activity by improving the tubulin binding affinity on the basis of a potential binding site nearby colchicine domain

Wei Zhao [a, 1], Long He [b, 1], Tian-Le Xiang [c] and Ya-Jie Tang [a, b, *]

[a] *State Key Laboratory of Microbial Technology, Shandong University, Qingdao 266237, China*

[b] *Hubei Key Laboratory of Industrial Microbiology, Hubei Provincial Cooperative Innovation Center of Industrial Fermentation, Key Laboratory of Fermentation Engineering (Ministry of Education), Hubei University of Technology, Wuhan 430068 China*

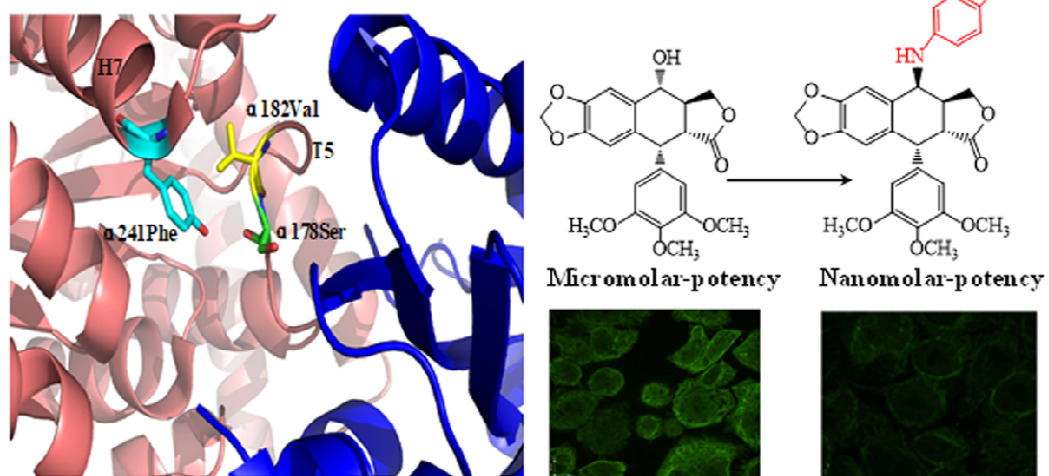[c] *No.11 Middle School of Wuhan, Wuhan 430068 China*

*Corresponding author. Tel. & Fax: +86-27-5975.0491 Email: yajietang@sdu.edu.cn

[1] These authors contributed equally to this work

CONFLICT OF INTEREST: No potential conflicts of interest were disclosed.

1

ABSTRACT

1 The colchicine binding site of tubulin is an attractive molecular target domain for cancer therapies.

2 However, there was no FDA approved drug for targeting colchicine domain. Our previous

3 crystallography discovered that a potential binding site of αT5 loop-αH7 nearby colchicine domain was

4 beneficial for introducing affinity fragment. In this work, benzo heterocycles (i.e., indole, indazole and

5 quinoline) with the high affinity ability of αT5 loop-αH7 were chosen as affinity fragment to modify

6 the molecule structure of podophyllotoxin for improving the tubulin binding affinity. 4β-*NH*-(benzo

7 heterocycles)-4-desoxy-podophyllotoxin were synchronously located at α/β interface of tubulin through

8 providing affinity fragment to αT5 loop-αH7 (i.e., α178Ser, α182Val, α241Phe) and colchicine domain

9 (i.e., β241Cys, β124ASP). 4β-*NH*-(6″-aminoindole)-4-desoxy-podophyllotoxin not only exhibited

10 nanomolar antitumor potency *in vitro* but also destroyed solid tumor growth without lethal toxicity *in*

11 *vivo*. The correctness of rational drug design was strictly demonstrated by bioactivity test.

12

13 **Keywords:** tubulin, colchicine domain, podophyllotoxin, binding affinity, nanomolar-potency

14 antitumor activity.

15

1. Introduction

Tubulin is a key component of the cytoskeletal network and an attractive molecular target for chemotherapeutic agents to treat cancer [1]. The tubulin heterodimer contains at least three distinct drug binding sites: the paclitaxel, vinblastine, and colchicine binding domain [2, 3]. Currently, for the paclitaxel and vinblastine domain, drugs were in current use in clinical oncology. Until now, no colchicine binding domain inhibitor was approved by FDA in anticancer therapy. Colchicine itself binds to tubulin, but the weak affinity hampered its activity and limited use in the clinic [4]. Many structure-based drugs design studies have been performed to discover new tubulin inhibitors with high affinity. However, many small molecule inhibitors target colchicine binding domain were published as a similar binding model: 1. the trimethoxyphenyl ring was embedded in the hydrophobic pocket (van der Waals contact with β352Lys, β350Asn, β318Val); 2. the methoxy group at para-position was involved in a hydrogen bond interaction with the thiol group of βCys241 [5, 6]. Although the above amino acid residues appeared to be crucial, the affinity was weak for tubulin inhibitor. Therefore, it was essential that new binding sites were introduced by domain analysis for discovering excellent antitumor drugs with superior affinity.

Podophyllotoxin (PTOX) was well-known for its potent cytotoxic activities against various cancer cell lines by competitive binding to the colchicine binding domain [7]. In our previous work, a binding model of the colchicine domain was found in the complexes of tubulin and 4β-(1,2,4-triazol-3-ylthio)-4-deoxypodophyllotoxin with superior antitumor activity. The crystal structures of complexes showed a binding site nearby colchicine domain, αT5 loop of tubulin was a potential binding site to be conducive to improve the affinity of tubulin with podophyllotoxin [8].

In this work, on the basis of αT5 loop-αH7 and colchicine binding domain, a class of benzo-heterocycles substituted podophyllotoxin derivatives was designed and synthesized for discovering novel therapeutic agents with nanomolar-potency activity by modifying the molecule

3

40   structure. Structure-activity relationships and target protein affinity indicated that

41   4β-*NH*-(6-aminoindole)-4-desoxy-podophyllotoxin could be explored as a multi-binding antitumor

42   drug. We described an important class of anti-tumor agents, their determinants on tubulin binding

43   affinity, and paved the way for further investigation into the efficacy of these drugs anti-tumor agents.

44   **RESULTS**

45   **Drug design and synthesis of 4β-*NH*-(benzo heterocycle)-podophyllotoxin derivatives.** According

46   to our previous the X-ray crystallology of 4β-(1,2,4-triazol-3-ylthio)-4-deoxypodophyllotoxin in

47   tubulin complex (5JCB) [8], podophyllotoxin skeleton of

48   4β-(1,2,4-triazol-3-ylthio)-4-deoxypodophyllotoxin mainly hydrophobic contacts with colchicine

49   binding domain by four hydrogen bond (Fig. 1A). Most importantly, the α-T5 loop in the α-tubulin was

50   directly bound by triazole of 4β-(1,2,4-triazol-3-ylthio)-4-deoxypodophyllotoxin. There were two

51   mainly hydrogen bonds formed between the αSer178 of αT5 loop and the triazole group of

52   4β-(1,2,4-triazol-3-ylthio)-4-deoxypodophyllotoxin. Notably, after surface treatment of α-tubulin, Fig.

53   1B clearly showed that αT5 and αH7 formed a pocket of 3.9 Å×5.2 Å×2.7 Å, which was an potential

54   binding site for inducing a series of affinity fragment at C-4 site of podophyllotoxin. The amino acid

55   residues indicated that αSer178, α182Val at αT5 and α241Phe at αH7 could provide affinity of

56   hydrogen bonds and conjugation interaction, respectively (Fig. 1C and 1D).

57   According to the potential binding site near colchicine binding domain, benzo heterocycles

58   containing oxygen, sulfur, or nitrogen atom were conducive to improve the affinity of α178Ser,

59   α182Val, and α241Phe in complex with podophyllotoxin by binding hydrogen bonds and conjugation

60   interaction (Fig. 2). The comparative molecular field analysis models showed that

61   electron-withdrawing substituents at the C-4 position of podophyllotoxin (PTOX) would enhance the

62   affinity of tubulin [9]. The indole skeleton was a scaffold that probably represents one of the most

63   important structural subunits for the discovery of new drug candidates [10]. Several indole-based

64 tubulin inhibitors have shown promising activity in preclinical studies [11, 12]. A number of tubulin

65 polymerization inhibitors, such as arylthioindoles [13], aroylindoles [14], and so on contained at least

66 one indole skeleton. Similarly, indazole and quinolone were the most frequently utilized heterocycles

67 skeleton among U.S. FDA approved drugs [15]. Indazole and quinoline scaffold were important

68 structural skeleton for the development of new antitumor drugs that function by cell cycle arrest,

69 apoptosis, inhibition of angiogenesis, disruption of cell migration and modulation [16, 17]. More

70 importantly, indole, indazole and quinolone scaffolds were the core structures of benzo heterocycles

71 containing oxygen, sulfur, or nitrogen atom, which were potential binding fragment with α178Ser,

72 α182Val, and α241Phe, which indicates that these heterocycles constitute a group of potent antitumor

73 drugs.

74   Accordingly, 12 benzo-heterocycles substituted PTOX derivatives was designed for discovering

75 novel therapeutic tubulin agents with nanomolar-potency activity. As shown in Table 1, for convenience

76 of comparison and screening, Compounds **1-12** were found to bind the active site between α and

77 β-tubulin by molecular docking. The distances of hydrogen bonds with α178Ser, α182Val, and α241Phe

78 was around 2.0-2.9 Å, 1.7-3.5 Å, and 1.6-2.4 Å, respectively (Fig. S1). The carbonyl oxygen of some

79 compounds was located in the oxyanion hole formed by the backbone nitrogen of β241Cys. The

80 oxygen atom at E-4′ position of some compounds formed hydrogen bond with β241Cys, β124ASP.

81 This result indicated all of the designed Compounds **1-12** possessed affinities with tubulin.

82   The docking data of the estimated free binding energy (ΔG), estimated inhibition constant (Ki),

83 hydrogen bonds and conjugated bonds were collected. The thermodynamic potential ΔG was used to

84 characterize the maximum energy of reversible binding in a thermodynamic system when compounds

85 targeted protein process. Compared with PTOX and colchicine, both of a higher absolute value of ΔG

86 and a lower Ki value were used to as a screening standard of target compound. As shown in Table 1, the

87 binding affinity of Compounds **1-12** (ΔG of 10.03-12.34 -kcal/mol, the Ki values of 0.01-0.12 μM)

88   were stronger than both PTOX (ΔG of 8.97 -kcal/mol, the Ki value of 0.27 µM) and Colchicine (ΔG of

89   9.57 -kcal/mol, the Ki value of 0.11 µM).

90   Taking the above rational analysis into consideration for drug design, heterocycles, including

91   indole, indazole, and quinolone linked via the C-NH bond at the C-4 position of PTOX. As shown in

92   Fig. 3, 12 new 4β-NH-(benzo heterocycle)-podophyllotoxin derivatives (i.e., Compounds **1-12**) were

93   synthesized by using our previously reported synthetic methodology of amino nucleophilic reaction

94   [18]. The intermediates 4β-iodopodophyllotoxin was synthesized by employing KI and BF_3OEt_2 in

95   CH_3CN. 4β-iodopodophyllotoxin were highly reactive and susceptible to nucleophilic attack in the

96   presence of any moisture. The crude indole-, indazole-, and quinolone-substituted podophyllotoxin

97   derivatives could be generated from the intermediates by employing $BaCO_3$ and Triethylamine (TEA)

98   in tetrahydrofuran (THF). The resulting mixture was filtered and evaporated to afford the crude

99   4β-NH-anilino-substituted podophyllotoxin congeners, which was further purified by high performance

100 liquid chromatography with methanol/water (40:60 v/v) to give the target compounds (> 95% pure). All

101 synthesized compounds were characterized by ^{1}H NMR, ^{13}C NMR and mass spectrometry (the data are

102 shown in the experimental section).

103 **Activity evaluation *in vitro*.** Compounds **1-12** were assessed by using the MTT assay. Four human

104 tumor cell lines (human liver carcinoma cells (HepG2), human cervical carcinoma cells (HeLa), human

105 lung cancer cells (A549), and human breast cancer cells (MCF7)) were selected for antitumor activity

106 assays. In addition, four normal human cell lines (human liver cells (HL7702), immortalized human

107 cervical epithelial cells (H8), human breast epithelial cells (HMEC), and human fetal lung fibroblast

108 cells (MRC-5)) were selected for cytotoxicity assays. The clinical microtubule polymerization inhibitor

109 nocodazole (Ncz), podophyllotoxin clinical drug etoposide (VP-16), PTOX, and DMEP were used as

110 positive controls. As shown in Table 2, most of the 4β-*NH*-nitrogen-containing benzo-fused

111 heterocyclic podophyllotoxin derivatives exhibited higher activities against tumor cells than Ncz,

112   VP-16,   PTOX,   and   DMEP.   Surprisingly,   the IC_{50} values   of

113   4β-*NH*-(6″-aminoindole)-4-desoxy-podophyllotoxin   (Compound   **3**)   and

114   4β-*NH*-(5″-aminoindazole)-4-desoxy-podophyllotoxin   (Compound   **6**)   reached

115   nanomolar-concentration levels. The IC_{50} values of Compound **3** against HepG-2, HeLa, A549, and

116   MCF-7 cell lines were 100, 80, 80, and 70 nM, respectively, which were significantly lower (by three

117   orders of magnitude) than the micromolar IC_{50} values of PTOX and VP-16 (Table 2). The antitumor

118   activity of Compound **3** was significantly higher than that of Ncz (with IC_{50} values of 400, 300, 200,

119   and 200 nM). In addition, most of the 4β-*NH*-heterocyclic podophyllotoxin derivatives exhibited

120   sufficiently low cytotoxicity against normal liver cells (Table 2). For example, the IC_{50} values of

121   Compound **3** against normal liver cells HL7702, H8, MRC-5, and HMEC were 94.6, 84.5, 69.1, and

122   61.6 µM, respectively, which indicated a lower cytotoxicity than that of Ncz, etoposide, and PTOX.

123   Notably, PTOX derivatives exhibited superior potential antitumor activities than those of the DMEP

124   derivatives among podophyllotoxin derivatives substituted with nitrogen-containing benzo-fused

125   heterocycles. Remarkably, the position of the C-NH substituent on the phenyl ring of the heterocycle

126   significantly influenced the antitumor activity and cytotoxicity against normal liver cell lines. For

127   example, the antitumor activity of 6-aminoindole-substituted PTOX exhibited the strongest activity

128   among   4-aminoindole-,   5-aminoindole-,   and   7-aminoindole-substituted   derivatives.

129   5-Aminoindole-substituted PTOX exhibited more potent activity than the 4-aminoindole- and

130   7-aminoindole-substituted derivatives. We found that if the C-NH substitution was in an electron poor

131   region,   the   antitumor   activity   was   improved.   Similar   results   were   observed   for   other

132   nitrogen-containing benzo-fused heterocyclic substitution patterns (Table 2). Finally, podophyllotoxin

133   derivatives substituted with five-membered nitrogen-containing benzo-fused heterocycles (i.e., indole

134   and indazole) generally showed better antitumor activities relative to their six-membered ring

135   counterparts. In summary, by rationally designing drugs and evaluating their activities *in vitro*,

7

136 Compound **3** and **6**, which show nanomolar antitumor potency, were identified for further investigation

137 of their pharmacological and biological mechanisms.

138 **Cell cycle arrest.** As shown in Fig. 4, accumulation of 50% of the cells in the G_2/M phase was

139 observed in MCF-7 treated with Compound **3** for 24 h at 100 nM, while the mitotic population was

140 only 20% in the untreated cells. The percentage of cells in the G_2/M phase increased to 90% after

141 incubation in 250 and 500 nM of Compound **3**. Interestingly, when MCF-7 cells were treated with

142 Compound **6** at a concentration of 250 nM, after 24 h, the population of G_2/M cells decreased from

143 80% to 45%. A similar trend was found for concentrations above 250 nM, suggesting that the release of

144 cells induced mitotic block. Compared to Compound **3** and **6**, etoposide, which arrested the cell cycle at

145 the G_2/M phase only at a concentration of 10 µM, was significantly less potent in cell cycle arrest. In

146 addition, similar results were observed in A549 and HeLa cancer cell lines treated with Compound **3**

147 and **6** (Fig. 4B and 4C). The data showed that Compound **3** and **6** could cause a gradual accumulation

148 of cells in the G_2/M phase of the cell cycle and induce apoptosis in a concentration- and time-dependent

149 manner.

150 **Apoptosis induction.** Compared to HepG2 cells, the tumor cell lines MCF-7, HeLa, and A549

151 exhibited strong drug sensitivity to Compound **3** and **6** in the above *in vitro* activity experiment.

152 Therefore, HeLa, MCF-7, and A549 cells were used as the cell models for the following study.

153 Compound **3** and **6** were tested in an induced-apoptosis assay using an annexin V/propidium iodide (PI)

154 staining apoptosis detection kit. The extent of apoptosis in MCF-7 cells was higher after treatment with

155 Compound **3** and **6** for 48 h than it was with VP-16 (Fig. 5A) at the same concentration. Compound **3**

156 at 250 nM induced apoptosis in approximately 93% of MCF-7 cells after 48 h. At the same

157 concentration, Compound **6** induced apoptosis in approximately 60% of cells. Almost no apoptosis was

158 observed in MCF-7 treated with 1 µM of VP-16. Interestingly, Compound **3** and **6** induced weak

159 apoptosis in MCF-7 cells prior to 24 h, but significantly induced apoptosis between 24 and 48 h. There

was a gradual and dose-dependent increase in the percentage (11.6, 10.5, 20.1, 93.5, 92.4, and 94.9%) of apoptotic MCF-7 cells when they were treated with Compound **3** for 48 h. Furthermore, a similar trend was observed in A549 and HeLa cancer cells (Fig. 5B and 5C) resulting in the cells swelling and then rupturing. These results confirmed that Compound **3** and **6** might significantly inhibit cell proliferation by inducing apoptosis in a time- and dose-dependent manner.

In summary, the indole- and indazole-substituted podophyllotoxin derivatives exhibited significantly more potency in G_2/M phase arrest and apoptosis induction than the podophyllotoxin clinical drug VP-16. Indole-substituted podophyllotoxin derivative Compound **3** showed higher potency than indazole-substituted podophyllotoxin derivative Compound **6** in the induction of cell death through apoptosis. The above results demonstrate that indole-substituted podophyllotoxin derivatives may induce apoptosis via an alternative mechanism, which we then investigated further as described below.

Binding affinity with tubulin. To further investigate the binding affinity of Compound **3** and **6** for tubulin, surface plasmon resonance (SPR) was employed. As shown in Fig. 6, the equilibrium dissociation constants (K_D values) of Compound **3** and **6** was 8.1 and 9.1 µM, respectively. The K_D values of PTOX and colchicine was 21.5 and 11.3 µM, respectively. The tubulin affinity of Compound **3** and **6** was approximately 2.7 and 2.2 times higher than that of PTOX and colchicine. These data indicate that the five-membered aromatic nitrogen heterocycles 6-aminoindole and 5-aminoindazole, which have higher electron densities around the nitrogen atom, could facilitate the stabilization of PTOX binding to tubulin. These data explained the higher antitumor activity of Compound **3** relative to that of Compound **6** in the *in vitro* MTT assay.

Tubulin Assembly. The degree of tubulin polymerization was evaluated through pellet mass formation. Inhibition curves were used to determine GI_{50}, which is the concentration that causes 50% growth inhibition. Fig. 7 clearly demonstrates that the microtubule polymerization inhibitory activities of PTOX, colchicine, nocodazole, Compound 3 and Compound 6 was gradually strengthens, respectively.

9

184 Compared with PTOX, colchicine, nocodazole, Compound 3 and 6 exhibition the stronger inhibition

185 ($GI_{50} < 0.1$ µM). The maximum inhibition ratio of Compound 3 and 6 was 88% and 79% respectively,

186 at a concentration of 2 µM.

187 **Inhibition of tubulin polymerization and phosphorylation of histone H3.** Compound **3** and **6**

188 clearly induced significant cell cycle accumulation in the G_2/M phase. Tubulin is essential for the

189 assembly of mitotic spindles [19, 20]. H2AX is a variant of an H2A core histone that produces

190 phosphorylation of histone variant H2AX (γH2AX) with phosphorylation in the vicinity of

191 double-strand DNA breaks upon treatment of the cells with drug or ionizing radiation [21]. The

192 presence of γH2AX was an accepted marker of the DSBs. Effect of Compound **3** and **6** on DNA

193 damage were studied by detecting fluorescence intensity of γH2AX. Therefore, whether the G_2/M cell

194 cycle arrest in cells treated with Compound **3** and **6** was due to an anti-tubulin effect by the same

195 mechanism as the colchicine was determined by immunofluorescence (Fig. 8).

196 Cells exhibited various phases of mitosis with no significant alteration, and cell shrinkage was

197 initiated after 24 h of incubation. In addition, when the cells were incubated with 500 nM of Compound

198 **3**, the cells were found to be contracted and rounded, suggesting complete inhibition of polymerization

199 of the tubulin cytoskeleton; the control cells (untreated) exhibited various phases of mitosis with

200 network-like structures of tubulin. Profound abnormalities in spindle-formation (micro-nucleated and

201 pro-metaphase with a ball or rosette of condensed DNA) were observed in cells treated with high

202 concentrations of 500 nM, resulting in disordered abnormal spindles and misalignment of

203 chromosomes. However, when the cells were treated with 500 nM PTOX, colchicine, and nocodazole,

204 respectively, the degree of damage to the tubulin network was less than what was seen with Compound

205 **3** and **6**. Analysis of tubulin morphology in the presence of different doses of Compound **3** and **6**

206 demonstrated that the normal morphology of the interphase tubulins in the presence of Compounds **3**

207 was not a result of partial inhibition of tubulin polymerization. These cell-based observations suggested

10

208 that Compound **3** and **6** were more effective against more dynamic spindles than against the less

209 dynamic interphase tubulins. In this assay, Compound **3** and **6** exhibited high affinity of tubulin. Taken

210 together, the results of these *in vitro* assays indicate that Compound **3** and **6** may be potent and selective

211 tubulin inhibitors.

212 **Antitumor effects of Compound 3 *in vivo*.** The effect of candidate drugs in animal models of cancer is

213 a good predictor of drug efficacy in humans, and tumor xenograft models are particularly useful. To

214 validate the potential antitumor effect of Compound **3** *in vivo*, nude mouse MCF-7 xenograft models

215 were established by subcutaneously injecting MCF-7 cells in the logarithmic phase into the right hind

216 leg of the mice. The results in Fig. 9 show that Compound **3** caused a considerable suppression of

217 tumor growth compared to the VP-16 groups. At the end of the observation period, the tumor volume

218 was maintained and slightly decreased in the VP-16 treatment group, but the mean final tumor had

219 completely collapsed in the Compound **3** treatment group. The average tumor weight of the VP-16

220 treatment groups was 0.834 ± 0.154 g (inhibitory rate: 43.2%), which was much less than that of the

221 Compound 3-treatment group (inhibitory rate: 89.6%). Compound **3** displayed potent anti-proliferative

222 activity *in vitro*, and its *in vivo* antitumor activity was obvious compared to that of the VP-16 treated

223 group.

224 **3. Discussion**

225 This work aimed to develop novel lead compounds with nanomolar antitumor potencies through

226 rational structural design and analysis of structure-activity relationships. Screening of the 12 newly

227 synthesized compounds revealed 4β-*NH*-(6″-aminoindole)-4-desoxy-podophyllotoxin (Compound **3**)

228 had nanomolar-level antitumor activity. In addition, compared to the tubulin inhibitory drug

229 nocodazole, Compound **3** showed higher tubulin affinity and DNA damage. Interestingly, how

230 Compound **3** reached nanomolar antitumor potency was unclear. To open a new approach for drug

231 design, we tried to develop a drug design theory for podophyllotoxin using structure-activity

232 relationships.

233   First, N-heterocycles are common in pharmaceuticals and biologically active molecules [15]. Over

234 the past few years, there has been considerable interest in the development and pharmacology of

235 heteroaromatic organic compounds, such as benzimidazoles, benzothiazoles, indoles, acridines,

236 oxadiazoles, imidazoles, isoxazoles, pyrazoles, triazoles, quinolines and quinazolines, because of their

237 diverse activities. Nitrogen-containing heterocycles are among the most important structural

238 components of pharmaceuticals. These N-heterocyclic compounds produce anticancer effects in

239 different types of cancer through inhibition of cell growth and induction of cell differentiation and

240 apoptosis. Some N-heterocyclic compounds have been approved by the U.S. FDA [7]. One type of atomic

241 orbital comes from the mixing of two or more atomic orbitals of an isolated atom. Indole and indazole

242 have strong hybridization that can enhance the protein binding capacity of the drug molecules because

243 hybrid orbitals are assumed to be mixtures of atomic orbitals superimposed on each other in various

244 proportions. The reaction mechanisms of indole and indazole sometimes progress via classical bonding

245 with two atoms sharing two electrons. However, predicting bond angles in drug design with hybrid

246 orbital theory is not straightforward. Podophyllotoxin (PTOX) is a naturally occurring aryltetralin

247 cyclolignan that contains four consecutive chiral centers (labeled C-1, C-2, C-3, and C-4) and four

248 almost planar fused rings (labeled A, B, C, and D). Because of three methoxy groups were

249 electron-donating groups, the E ring exhibit positive electricity. As a mainly modification site, the

250 carbon atom of C-4 with a hydroxyl electron absorbing group is a carbocation. It is well known that the

251 electronegativity is the ability of atoms to attract bonding electrons in molecules. After modification of

252 electron-withdrawing group indole or indazole at C-4 site of PTOX, nitrogen atoms with high

253 electronegativity pulled the shared electrons to the other side, making the charge of PTOX molecule

254 unevenly distributed. As shown in Fig. 10, compared with PTOX, the electron cloud of

255 4β-NH-(6-aminoindole)-4-desoxy-podophyllotoxin   or

256 4β-NH-(6-aminoindole)-4-desoxy-podophyllotoxin significantly aggregated together due to stronger

257 electron-withdrawing effect. More dipoles bonds were formed, and such bonds were polar bonds. The

258 dipole   of   4β-NH-(6-aminoindole)-4-desoxy-podophyllotoxin   or

259 4β-NH-(6-aminoindole)-4-desoxy-podophyllotoxin was also higher than PTOX. The whole of the

260 outside of PTOX molecule was somewhat negative. So, in this work, indole and indazole could

261 enhance the electronegativity of podophyllotoxin, which might be further improve its tubulin affinity.

262   Second, indole and indazole could significantly enhance antitumor activities and alter the

263 conformation of molecules to improve the binding affinities for the target protein tubulin. The

264 theoretical binding mode of Compound **3** and **6** at the colchicine binding domain in the tubulin dimer

265 was investigated by using tubulin (PDB code: 5JCB). An overview of the binding modes of Compound

266 3 and 6 in the αβ-tubulin dimer did show overlap with the colchicine binding domain. As shown in Fig.

267 11, a detailed docking model of Compound **3** revealed the E-ring of PTOX was located at the pocket of

268 the β-tubulin and the hydroxyl group was positioned toward the α-tubulin. Accordingly, indole and

269 indazole substituents on C-4 site were bound in the same direction as the hydroxyl group. The indole

270 group of Compound **3** generates two important H-bond with the side chain of α-tubulin (α178Ser) and a

271 π-π interaction with α352Lys. Instead, the indazole docked model of Compound **6** showed a π-π

272 interaction with α375Phe of and an interaction with the α238Val side chains, which was consistent with

273 the previously discussed SPR results. Several indole analogs are highly cytotoxic against many tumor

274 cell lines at concentrations similar to those of several well-known anti-mitotic agents, such as

275 colchicine, vincristine, vinblastine, and paclitaxel. For most of the tested compounds, the experimental

276 data are consistent with the inhibition of tubulin polymerization through binding at the

277 colchicine-binding site.

278   The structure-activity relationships of all the synthesized compounds were summarized. The

279 present discussion of podophyllotoxin derivatives focusses primarily on substitutions, additions and

different substitution module at the C-4 position. In general, meta-substitution at the C-4 position led to more potent compounds than ortho-substitution of the benzene ring. Analogs with five-membered heterocycles at the C-4 position were more potent than the corresponding six-membered heterocycle analogs.

4. Conclusion

For the first time, this work focused on the discovery of potent antitumor leading compounds with the nanomolar-potency activity by improving the tubulin binding affinity of podophyllotoxin (PTOX).

A potential binding site αT5 loop-αH7 close to colchicine domain was conducive to improve the affinity of tubulin with podophyllotoxin. Accordingly, benzo heterocycles with the affinity ability of αT5 loop (i.e., α178Ser, α182Val, and α241Phe) were chosen as functional modules to improve the tubulin binding affinity of PTOX. A total of 12 new 4β-(benzo heterocycles)-podophyllotoxin were designed and synthesized. Among these compounds, indole and indazole substituted PTOX derivatives exhibited higher tubulin binding affinity and stronger inhibition of microtubule polymerization. The equilibrium dissociation constants (K_D values) of Compound **3** and **6** was 8.1 and 9.1 μM, respectively. Compared with PTOX (the K_D values of 21.5 μM) and colchicine (the K_D values of 11.3 μM), the tubulin binding affinity of Compound **3** and **6** was approximately 2.7 and 2.2 times higher than that of PTOX and colchicine. The tubulin affinity and intracellular microtubule inhibition indicated that Compound 3 strongly bound to tubulin, resulting in the inhibition of microtubule polymerization. The correctness of colchicine domain structure-based drug design was strictly demonstrated by affinity tests.

The IC_{50} value of Compound **3** was 0.1±0.01, 0.08±0.0, 0.08±0.0, and 0.07±0.0 μM. The IC_{50} value of PTOX were 2.4±0.1, 6.9±0.1, 2.6±0.1, and 2.4±0.3 μM against HepG2, HeLa, A549 and MCF-7 cells, respectively. The IC_{50} value of parent molecular PTOX were 2.4±0.1, 6.9±0.1, 2.6±0.1, and 2.4±0.3 μM, and the IC_{50} value of colchicine was 5.8±3.8, 10.2±0.4, 9.7±0.2 and 14.3±0.5 μM. The

antitumor activity of Compound **3** significantly improved by 26-85 times than PTOX and 98-203 times than colchicine. Most noteworthy, Compound **3** not only exhibited nanomolar antitumor potency *in vitro* but also significantly destroyed solid tumor growth without lethal toxicity *in vivo*. Compound 3 induced tumor cell apoptosis and arrested cell cycle progression in the G_2/M phase at nanomolar concentrations level. Because of potent tubulin binding affinity and nanomolar-potency activity, Compounds **3** was a valuable leading compound for new drug development.

The structure-activity relationships indicated that benzo-heterocycles indole significantly provided the molecular hybridization on α-tubulin binding domain (i.e., α178Ser, α182Val, and α241Phe) and expanded binding model of PTOX to improve the tubulin binding affinities. The active sites of tubulin suggested that the docking of PTOX derivatives led to interaction with theα178Ser, α182Val, and α241Phe residue at the α-tubulin interface. When indoles or indazoles with dispersed hybrid orbitals were incorporated into the PTOX, there were significant improvements in the inhibition of tumor cell growth compared to PTOX and colchicine. These results show the importance of the benzo-heterocycle in the modification of PTOX derivatives displayed a dual-binding affinity on α and β-tubulin.

In conclusion, this work reported on discovery of leading compounds with nanomolar-potency antitumor activity by improving the tubulin binding affinity on the basis of a potential binding site nearby colchicine domain. A representative leading compound, Compound **3** exhibited potent antitumor on human tumor cells (i.e., HpeG2, HeLa, A549 and MCF-7) by synchronously targeting the α-tubulin binding site (i.e., α178Ser, α182Val, and α241Phe) and colchicine binding domain. Compound **3** not only exhibited nanomolar antitumor potency *in vitro* but also destroyed solid tumor growth without lethal toxicity *in vivo*. The correctness of rational drug design was strictly demonstrated by a bioactivity test.

5. Experimental section

General Chemistry. Analytical grade chemical reagents were used as purchased from commercial

328 sources (Aladdin, *J&K* and Sigma-Aldrich). Podophyllotoxin (1 mM, 1 equiv) and KI (1.5 mM, 1.5

329 equiv) were dissolved in CH_3CN (10 mL) at 0□ for 5 min. And then BF_3OEt_2 (3.5 mM, 3.5 equiv) was

330 slowly added dropwise under magnetic stirring. The mixture was stirred at room temperature for 1 h

331 and resulted in a brown solution. The reaction mixture was concentrated in vacuo to afford

332 4β-iodopodophyllotoxin (yield, 85%), respectively, which was unstable intermediates for the next step

333 of the synthesis leading to the final products. The indole intermediates (1 mM, 1 equiv) and amino

334 substituted precursors (1 mM, 1 equiv) were dissolved in THF. $BaCO_3$ (5 mM, 5 equiv) was added to

335 the mixture as an acid-binding agent. Triethylamine (TEA) was slowly added dropwise under magnetic

336 stirring. The samples were filtered with a 0.45 µm micropore filter and transferred to a sampling vial

337 for HPLC analysis. HPLC analysis was carried out on a Waters 600 Series HPLC system, equipped

338 with 2487 UV detector. An Akasil C18 column (5 µm, 4.6 mm × 150 mm) was used. Mobile phase was

339 methanol/water (40:60 v/v) and the pH was adjusted to 3.00 with formic acid. The HPLC oven

340 temperature was maintained at 45 °C, and the detection wavelength was 230 nm or 219 nm. The flow

341 rate was 0.8 ml/min. All ^{1}H and ^{13}C NMR spectra were recorded on an Agilent (400 MHz) NMR

342 spectrometer with tetramethylsilane as the internal standard (δ ppm). The following abbreviations are

343 used: singlet (s), doublet (d), triplet (t) and multiplet (m). Mass spectroscopic data were obtained on a

344 Shimadzu ESI-MS instrument.

345 *4β-NH-(4′′-aminoindole)-4-desoxy-podophyllotoxin (1).* White powder, yield: 61%; purity: 98%; mp:

346 186-188 °C; ^{1}H NMR (400 MHz, CDCl$_3$): δ 8.42 (s, 1H), 7.63 (d, *J*=8.05 Hz, 1H), 7.25 (m, 1H), 6.77 (s,

347 1H), 6.72 (d, *J*=12.31 Hz, 2H), 6.45 (s, 1H), 6.37 (s, 1H), 6.34 (s, 2H), 5.95 (dd, *J*=5.20 Hz, 2H), 4.82

348 (dd, 8.02, 16.04 Hz, 1H), 4.66 (d, *J*=4.35 Hz, 1H), 4.30 (t, 1H), 4.08-3.95 (m, 1H), 3.80 (s, 3H), 3.78 (s,

349 6H), 3.20 (dd, *J*=12.0 Hz, 1H), 3.05-2.90 (m, 1H). ^{13}C NMR (100 MHz, CDCl$_3$): δ 175.45, 148.28,

350 147.42, 146.40, 139.88, 137.32, 134.26, 131.64, 131.41, 130.67, 122.32, 121.63, 120.88, 109.78,

351 109.17, 108.06, 102.39, 101.45, 92.74, 69.23, 56.50, 53.32, 43.45, 42.11, 38.80. HRMS (ESI) (*m/z*):

352   [M+H]$^+$, $C_{30}H_{28}N_2O_7$, calculated, 529.55; found, 529.57. Purity: 96.0% (by HPLC).

353   *4β-NH-(5''-aminoindole)-4-desoxy-podophyllotoxin (2).* White powder, yield: 45%; purity: 98%; mp:

354   199-201 ^{o}C; ^{1}H NMR (400 MHz, CDCl$_3$): δ 8.33 (s, 1H), 7.40 (d, *J*=8.05 Hz, 1H), 7.06 (m, 1H), 6.71 (s,

355   1H), 6.52 (d, *J*=12.11 Hz, 2H), 6.44 (s, 1H), 6.37 (s, 1H), 6.35 (s, 2H), 5.96 (dd, *J*=5.20 Hz, 2H), 4.82

356   (dd, 8.1, 16.2 Hz, 1H), 4.70 (d, *J*=.35 Hz, 1H), 4.35 (t, 1H), 4.06-3.94 (m, 1H), 3.77 (s, 3H), 3.75 (s,

357   6H), 3.16 (dd, *J*=12.0 Hz, 1H), 3.04-2.93 (m, 1H). ^{13}C NMR (100 MHz, CDCl$_3$): δ 174.25, 148.04,

358   147.38, 146.64, 139.74, 137.22, 134.01, 131.62, 131.41, 130.58, 122.79, 121.82, 120.95, 109.85,

359   109.17, 108.05, 102.45, 101.47, 92.76, 69.27, 56.52, 53.47, 43.45, 42.11, 38.80. HRMS (ESI) (*m/z*):

360   [M+H]$^+$, $C_{30}H_{28}N_2O_7$, calculated, 529.54; found, 529.55. Purity: 98.0% (by HPLC).

361   *4β-NH-(6''-aminoindole)-4-desoxy-podophyllotoxin (3).* Yellow powder, yield: 33%; purity: 97%; mp:

362   192-193 ^{o}C; ^{1}H NMR (400 MHz, CDCl$_3$): δ 8.13 (s, 1H), 7.43 (d, *J*=8.45 Hz, 1H), 7.03 (m, 1H), 6.77 (s,

363   1H), 6.55 (d, *J*=36.31 Hz, 2H), 6.43 (s, 1H), 6.36 (s, 1H), 6.33 (s, 2H), 5.93 (dd, *J*=5.70 Hz, 2H), 4.81

364   (dd, 10.08, 20.04 Hz, 1H), 4.68 (d, *J*=.35 Hz, 1H), 4.34 (t, 1H), 4.06-3.95 (m, 1H), 3.79 (s, 3H), 3.77 (s,

365   6H), 3.18 (dd, *J*=14.0 Hz, 1H), 3.03-2.94 (m, 1H). ^{13}C NMR (100 MHz, CDCl$_3$): δ 175.25, 148.08,

366   147.48, 146.44, 139.94, 137.12, 134.06, 131.69, 131.11, 130.88, 122.29, 121.62, 120.89, 109.80,

367   109.17, 108.07, 102.41, 101.45, 92.75, 69.26, 56.50, 53.32, 43.42, 42.01, 38.82. HRMS (ESI) (*m/z*):

368   [M+H]$^+$, $C_{30}H_{28}N_2O_7$, calculated, 529.52; found, 529.55. Purity: 97.4% (by HPLC).

369   *4β-NH-(7''-aminoindole)-4-desoxy-podophyllotoxin (4).* White powder, yield: 37%; purity: 98%; mp:

370   204-206 ^{o}C; ^{1}H NMR (400 MHz, CDCl$_3$): δ 8.10 (s, 1H), 7.42 (d, *J*=8.25 Hz, 1H), 7.00 (m, 1H), 6.74 (s,

371   1H), 6.48 (d, *J*=16.30 Hz, 2H), 6.40 (s, 1H), 6.34 (s, 1H), 6.30 (s, 2H), 5.91 (dd, *J*=4.70 Hz, 2H), 4.81

372   (d, 12.04 Hz, 1H), 4.65 (d, *J*=.35 Hz, 1H), 4.32 (t, 1H), 4.09-3.97 (m, 1H), 3.80 (s, 3H), 3.78 (s, 6H),

373   3.15 (dd, *J*=14.0 Hz, 1H), 3.05-2.96 (m, 1H). ^{13}C NMR (100 MHz, CDCl$_3$): δ 175.05, 148.02, 147.44,

374   146.43, 139.84, 137.42, 134.16, 131.62, 131.10, 130.85, 122.27, 121.60, 120.86, 109.81, 109.13,

375   108.00, 102.40, 101.44, 92.72, 69.23, 56.47, 53.3., 43.46, 42.00, 38.76. HRMS (ESI) (*m/z*): [M+H]$^+$,

376 $C_{30}H_{28}N_2O_7$, calculated, 529.53; found, 529.54. Purity: 98.5% (by HPLC).

377 *4β-NH-(4″-indazolamine)-4-desoxy-podophyllotoxin (5)*. White powder, yield: 28%; purity: 98%; mp:

378 255-257 $^{\circ}$C; ^{1}H NMR (400 MHz, CDCl$_3$): δ 8.10 (s, 1H), 7.55 (d, *J*=8.0 Hz, 1H), 7.49 (s, 1H), 6.72 (s,

379 1H), 6.72 (m, 2H), 6.64 (d, *J*=4 Hz, 1H), 6.48 (s, 1H), 6.32 (s, 2H), 5.95 (dd, *J*=6.0 Hz, 2H), 4.69 (s,

380 1H), 4.56 (d, *J*=4.0 Hz, 1H), 4.45 (t, 1H), 3.95-3.91 (m, 1H), 3.80 (s, 3H), 3.76 (s, 6H), 3.25 (dd,

381 *J*=14.0 Hz, 1H), 3.10-2.99 (m, 1H). ^{13}C NMR (100 MHz, CDCl$_3$): δ 175.25, 152.55, 148.11, 147.52,

382 142.30, 137.12, 135.35, 135.21, 133.20, 131.62, 130.80, 129.85, 118.22, 111.43, 109.67, 109.23,

383 108.35, 101.50, 98.04, 69.16, 60.82, 56.26, 53.38, 43.62, 42.02, 38.82. HRMS (ESI) (*m/z*): [M+H]$^+$,

384 $C_{29}H_{27}N_3O_7$, calculated, 530.54; found, 530.52. Purity: 97.0% (by HPLC).

385 *4β-NH-(5″-indazolamine)-4-desoxy-podophyllotoxin (6)*. White powder, yield: 41%; purity: 99%; mp:

386 204-206 $^{\circ}$C; ^{1}H NMR (400 MHz, CDCl$_3$): δ 7.89 (s, 1H), 7.32 (d, *J*=8.0 Hz, 1H), 7.39 (s, 1H), 6.76 (s,

387 1H), 6.75-6.73 (m, 2H), 6.69 (d, *J*=4 Hz, 1H), 6.50 (s, 1H), 6.33 (s, 2H), 5.93 (dd, *J*=6.0 Hz, 2H), 4.68

388 (s, 1H), 4.58 (d, *J*=4.0 Hz, 1H), 4.42 (t, 1H), 3.94-3.90 (m, 1H), 3.80 (s, 3H), 3.74 (m, 6H), 3.20 (dd,

389 *J*=14.0 Hz, 1H), 3.08-2.99 (m, 1H). ^{13}C NMR (100 MHz, CDCl$_3$): δ 175.05, 152.57, 148.16, 147.57,

390 142.36, 137.17, 135.40, 135.26, 133.25, 131.66, 130.83, 129.90, 118.12, 111.33, 109.87, 109.13,

391 108.29, 101.51, 98.04, 69.12, 60.75, 56.25, 53.36, 43.58, 41.97, 38.77. HRMS (ESI) (*m/z*): [M+H]$^+$,

392 $C_{29}H_{27}N_3O_7$, calculated, 530.54; found, 530.58. Purity: 96.6% (by HPLC).

393 *4β-NH-(6″-indazolamine)-4-desoxy-podophyllotoxin (7)*. White powder, yield: 46%; purity: 98%; mp:

394 190-192 $^{\circ}$C; ^{1}H NMR (400 MHz, CDCl$_3$): δ 8.01 (s, 1H), 7.30 (d, *J*=8.0 Hz, 1H), 7.35 (s, 1H), 6.71 (s,

395 1H), 6.73 (m, 2H), 6.64 (d, *J*=4 Hz, 1H), 6.47 (s, 1H), 6.30 (s, 2H), 5.91 (dd, *J*=4.90 Hz, 2H), 4.64 (s,

396 1H), 4.52 (d, *J*=4.0 Hz, 1H), 4.37 (t, 1H), 3.91 (m, 1H), 3.80 (s, 3H), 3.78 (m, 6H), 3.24 (dd, *J*=14.0

397 Hz, 1H), 3.04 (m, 1H). ^{13}C NMR (100 MHz, CDCl$_3$): δ 175.15, 152.50, 148.56, 147.77, 142.46, 137.24,

398 135.30, 135.21, 133.29, 131.62, 130.82, 129.94, 118.02, 111.13, 109.85, 109.12, 108.25, 101.50, 98.01,

399 69.10, 60.74, 56.25, 53.34, 43.51, 42.04, 38.79. HRMS (ESI) (*m/z*): [M+H]$^+$, $C_{29}H_{27}N_3O_7$, calculated,

400   530.55; found, 530.52. Purity: 98.2% (by HPLC).

401   *4β-NH-(6″-indazolamine)-4′-demethyl-4-desoxy-podophyllotoxin* **(7′)**. White powder, yield: 52%;

402   purity: 97%; mp: 189-192 ^{o}C; ^{1}H NMR (400 MHz, CDCl$_3$): δ 7.98 (s, 1H), 7.31 (d, *J*=8.80 Hz, 1H),

403   7.68 (m, 2H), 6.62 (d, *J*=4.65 Hz, 1H), 6.50 (s, 1H), 6.49 (d, *J*=4 Hz, 1H), 6.41 (s, 1H), 6.32 (s, 2H),

404   5.91 (dd, *J*=4.30 Hz, 2H), 4.61 (t, *J*=4.44 Hz, 1H), 4.50 (d, *J*=4.92 Hz, 1H), 4.42 (t, *J*=3.94 Hz, 1H),

405   4.00 (m, 1H), 3.85 (d, *J*=4.26 Hz, 1H), 3.79 (s, 6H), 3.25 (dd, *J*=11.99 Hz, 1H), 3.05-2.99 (m, 1H). ^{13}C

406   NMR (100 MHz, CDCl$_3$): 175.20, 148.06, 147.54, 146.44, 142.32, 135.14, 134.03, 133.22, 131.80,

407   130.71, 130.59, 123.82, 118.10, 111.27, 109.99, 109.02, 108.00, 101.47, 98.08, 69.13, 56.45, 53.42,

408   43.45, 42.17, 38.73. HRMS (ESI) (*m/z*): [M+H]$^+$,C$_{28}$H$_{35}$N$_3$O$_7$, calculated, 516.52; found, 516.55. Purity:

409   97.0% (by HPLC).

410   *4β-NH-(7″-indazolamine)-4-desoxy-podophyllotoxin* **(8)**. White powder, yield: 55%; purity: 98%; mp:

411   203-205 ^{o}C; ^{1}H NMR (400 MHz, CDCl$_3$): δ 7.80 (s, 1H), 7.39 (s, 1H), 7.30 (d, *J*=4.0 Hz, 1H), 6.71 (s,

412   1H), 6.73 (m, 2H), 6.62 (d, *J*=4.01 Hz, 1H), 6.43 (s, 1H), 6.30 (s, 2H), 5.85 (dd, *J*=6.0 Hz, 2H), 4.65 (s,

413   1H), 4.51 (d, *J*=4.10 Hz, 1H), 4.40 (t, 1H), 3.92 (m, 1H), 3.72 (s, 3H), 3.79 (m, 6H), 3.22 (dd, *J*=14.0

414   Hz, 1H), 3.05-2.99 (m, 1H). ^{13}C NMR (100 MHz, CDCl$_3$): δ 174.95, 152.27, 148.36, 147.47, 142.32,

415   137.12, 135.41, 135.20, 133.21, 131.59, 130.80, 129.82, 118.10, 111.28, 109.84, 109.10, 108.22,

416   101.50, 98.08, 69.10, 60.79, 56.28, 53.39, 43.58, 42.05, 38.79. HRMS (ESI) (*m/z*): [M+H]$^+$,

417   C$_{29}$H$_{27}$N$_3$O$_7$, calculated, 530.54; found, 530.53. Purity: 95.6% (by HPLC).

418   *4β-NH-(5″-aminoquinoline)-4-desoxy-podophyllotoxin* **(9).** White powder, yield: 48%; purity: 98%; mp:

419   214-216 ^{o}C; ^{1}H NMR (400 MHz, CDCl$_3$): δ 8.84 (d, *J*=3.63 Hz, 1H), 8.16 (d, *J*=8.45 Hz, 1H),

420   7.58-7.52 (m, 2H), 7.29 (dd, *J*=8.53 Hz, 1H), 6.75 (s, 1H), 6.56 (d, *J*=6.87 Hz, 1H), 6.53 (s, 1H), 6.32

421   (s, 2H), 5.94 (d, *J*=4.58 Hz, 2H), 4.91 (t, *J*=4.43 Hz, 1H), 4.69 (d, *J*=5.04 Hz, 1H), 4.61 (d, *J*=4.89 Hz,

422   1H), 4.41 (t, *J*=7.98 Hz, 1H), 3.90 (dd, *J*=10.34 Hz, 1H), 3.79 (s, 3H), 3.74 (s, 6H), 3.24 (dd, *J*=14.03

423   Hz, 1H), 3.13-3.04 (m, 1H). ^{13}C NMR (100 MHz, CDCl$_3$): δ 174.50, 152.60, 150.30, 149.14, 148.42,

424 147.76, 142.86, 137.20, 135.02, 132.12, 130.10, 130.04, 128.68, 119.73, 119.59, 117.92, 109.98,

425 109.17, 108.22, 103.95, 101.61, 68.92, 60.75, 56.25, 52.62, 43.59, 42.09, 38.56. HRMS (ESI) (*m/z*):

426 [M+H]$^+$, C$_{31}$H$_{28}$N$_2$O$_7$, calculated, 541.56; found, 541.53. Purity: 99.5% (by HPLC).

427 *4β-NH-(6″-aminoquinoline)-4-desoxy-podophyllotoxin (10)*. White powder, yield: 44%; purity: 98%;

428 mp: 187-189 ^{o}C; ^{1}H NMR (400 MHz, CDCl$_3$): δ 8.64 (d, *J*=3.26 Hz, 1H), 7.91 (t, *J*=8.44 Hz, 2H), 7.30

429 (dd, *J*=8.28 Hz, 1H), 7.06 (dd, *J*=9.02 Hz, 1H), 6.79 (s, 1H), 6.65 (d, *J*=2.43 Hz, 1H), 6.54 (s, 1H),

430 6.33 (s, 2H), 5.96 (d, *J*=6.47 Hz, 2H), 4.83 (m, 1H), 4.62 (d, *J*=4.74 Hz, 1H), 4.44 (m, 1H), 4.28 (d,

431 *J*=5.96 Hz, 1H), 3.99 (m, 1H), 3.81 (s, 3H), 3.74 (s, 6H), 3.18 (dd, *J*=14.04 Hz, 1H), 3.13-3.04 (m, 1H).

432 ^{13}C NMR (100 MHz, CDCl$_3$): δ 174.56, 152.63, 148.40, 147.71, 146.79, 145.34, 143.38, 137.31,

433 134.99, 133.88, 131.88, 130.85, 130.03, 121.79, 120.86, 117.92, 109.96, 109.16, 108.31, 102.56,

434 101.60, 68.82, 60.75, 56.29, 52.62, 43.57, 42.01, 38.62. HRMS (ESI) (*m/z*): [M+H]$^+$, C$_{31}$H$_{28}$N$_2$O$_7$,

435 calculated, 541.18; found, 541.12. Purity: 98.0% (by HPLC).

436 *4β-NH-(7″-aminoquinoline)-4-desoxy-podophyllotoxin (11).* White powder, yield: 51%; purity: 98%;

437 mp: 197-199 ^{o}C; ^{1}H NMR (400 MHz, CDCl$_3$): δ 9.16 (s, 1H), 8.44 (d, *J*=8.0 Hz, 1H), 7.53-7.46 (m,

438 2H), 7.40 (d, *J*=8 Hz, 1H), 6.74 (s, 1H), 6.70 (d, *J*=4.1 Hz, 1H), 6.56 (s, 1H), 6.50 (s, 1H), 6.34 (s, 2H),

439 5.95 (t, 2H), 4.90 (t, 1H), 4.64 (t, 2H), 4.43 (t, 1H), 3.94-3.87 (m, 1H), 3.80 (s, 3H), 3.76 (m, 6H), 3.27

440 (dd, *J*=12.0 Hz, 1H), 3.16-3.09 (m, 1H). ^{13}C NMR (100 MHz, CDCl$_3$): δ 174.50, 152.94, 152.63,

441 148.52, 147.83, 142.39, 141.75, 137.26, 134.97, 135.15, 129.97, 127.79, 125.49, 117.49, 113.17,

442 110.06, 109.10, 108.26, 106.89, 101.65, 68.81, 60.76, 56.28, 52.56, 43.59, 42.09, 38.60. HRMS (ESI)

443 (*m/z*): [M+Na]$^+$, C$_{31}$H$_{28}$N$_2$O$_7$, calculated, 563.56; found, 563.58. Purity: 96.4% (by HPLC).

444 *4β-NH-(8″-aminoquinoline)-4-desoxy-podophyllotoxin (12).* Yellow powder, yield: 45%; purity: 98%;

445 mp: 195-197 ^{o}C; ^{1}H NMR (400 MHz, CDCl$_3$): δ 8.67 (dd, *J*=4.0 Hz, 1H), 8.08 (dd, *J*=4.0 Hz, 1H),

446 7.40-7.36 (m, 2H), 7.14 (d, *J*=8 Hz, 1H), 6.78 (s, 1H), 6.59 (d, *J*=7.52 Hz, 1H), 6.56 (s, 1H), 6.55 (s,

447 1H), 6.45 (d, *J*=6.77 Hz, 1H), 6.38 (s, 2H), 5.92 (dt, *J*=4.71 Hz, 2H), 4.87 (dd, *J*=6.39 Hz, 1H), 4.66 (d,

448 *J*=4.98 Hz, 1H), 4.43 (t, *J*=7.99 Hz, 1H), 3.97 (dd, *J*=10.74 Hz, 1H), 3.81 (s, 3H), 3.77 (s, 6H), 3.27

449 (dd, *J*=14.08 Hz, 1H), 3.16-3.07 (m, 1H). ^{13}C NMR (100 MHz, CDCl$_3$): δ 174.50, 152.59, 148.24,

450 147.58, 147.29, 144.05, 137.67, 137.22, 136.14, 135.32, 131.83, 130.48, 128.74, 127.42, 121.83,

451 115.34, 109.81, 109.51, 108.37, 104.10, 101.46, 68.95, 60.76, 56.28, 52.23, 43.68, 42.08, 39.00.

452 HRMS (ESI) (*m/z*): [M+H]$^+$, calcd for C$_{31}$H$_{28}$N$_2$O$_7$, 541.56; found, 541.52. Purity: 95.5% (by HPLC).

453 **Antitumor and cytotoxicity activity assay (MTT assay).** All human cell lines, namely, human liver

454 carcinoma cells (HepG2), human cervical carcinoma cells (HeLa), human lung cancer cells (A549),

455 human breast cancer cells (MCF7), human liver cells (HL7702), immortalized human cervical

456 epithelial cells (H8), human breast epithelial cells (HMEC), human fetal lung fibroblast cells (MRC-5),

457 were grown in T-25 flasks in a Thermo Scientific CO$_2$ incubator in a humidified environment at 37□

458 and 5% CO$_2$. Additionally, HeLa, HepG2, H8 and HL7702 cells were maintained in RPMI 1640

459 medium (Gibico, Thermo Fisher) containing 10% fetal calf serum (Sigma) and 1% penicillin

460 C/streptomycin (Biosharp), and A549, MCF-7, MRC-5 and HMEC were maintained in high-glucose

461 DMEM (HyClone^{TM}) containing 10% fetal calf serum and 1% penicillin C/streptomycin.

462 Compounds were assessed for cytotoxic activity *in vitro* against several cancer cell lines by MTT

463 assay. Freshly trypsinized cell suspensions in the logarithmic growth phase were seeded in a 96-well

464 microtiter plate (4000-12000 cells per well, based on the doubling time). The newly attached cells in

465 the 96-well microtiter plate were treated with varying concentrations compounds 1-24 (10-fold

466 dilutions starting from 100 μM to 10 nM, dissolved in DMSO (0.1% v/v) without effect on cell growth).

467 After 48 h of incubation with the test compounds, attached cells were treated with 100 μL of MTT (2

468 mg/mL) solution in the growth medium. The cells were incubated for an additional 4 h at 37°C until a

469 purple precipitate was visible. The purple formazan crystals were dissolved with 100 μL DMSO, and

470 the absorbance of each sample was measured at 492 nm using a microplate reader (Cytation 3, BioTek)

471 with Gen5 software (BioTek). All values presented in Table 1 are the average of triplicate experiments.

472   IC_{50} values were calculated using Orange 8 software.

473   **Analysis of cell apoptosis by flowcytometry.** Cellular apoptosis was measured by annexin V/PI

474   double staining using flowcytometry. Freshly trypsinized cell suspensions $(1\times10^5\text{-}1\times10^6)$ in the

475   logarithmic growth phase were seeded in a 6-well plate. After the cell lines had adhered to the plate,

476   they were treated with various concentrations of the synthesized compounds. The plates were incubated

477   for 48 h. The cells were incubated in cycles of 6 hours on and 6 hours off for a total of 48 h. The cells

478   were then collected by washing twice with PBS (0.5 mL), trypsinizing (100 µL) and centrifuging (1500

479   rpm, 5 min). Binding buffer suspension (500 µL) was added to resuspend the cells, and then the cells

480   were double stained with annexin V (1 µg/mL) and PI (0.5 µg/mL) in a Ca^{2+} enriched binding buffer

481   for 15 min in the dark at room temperature. Data were collected using a BD-C6 flow cytometer with

482   modes on 10,000 events for FL1 versus FL2 channels. Apoptosis rates were calculated by accumulating

483   early and late stage results. Experiments were repeated a minimum of three times.

484   **Cell cycle analysis by flowcytometry.** Cell cycle phase distribution was assessed by measuring the

485   cellular DNA content using PI staining. Freshly trypsinized cell suspensions $(1\times10^5\text{-}1\times10^6)$ in the

486   logarithmic growth phase were seeded in a 6-well plate. After the cell lines had adhered to the plate,

487   they were treated with various concentrations of the synthesized compounds (Compound 3 at

488   concentrations 10, 50, 100, 250, and 500 nM, and all other compounds at concentrations of 50, 100,

489   250, 500, and 1000 nM). The cells were incubated in cycles of 6 hours on and 6 hours off for a total of

490   48 h. The cells were then washed twice with pre-cooling PBS (Gibico, Phosphate-Buffered Saline),

491   trypsinized, collected by centrifugation for 5 min at 1500 rpm, fixed in 70% ethanol and stored at -20□

492   for at least 2 days. The cells were then stained with PI (50 µg/mL) for 30 min on ice in the dark. The

493   DNA content was measured by a BD-C6 flow cytometer (Becton Dickinson, USA) with modes on

494   10,000 events for FL2-A versus FL2-W. Cell cycle phase distributions (G_1, S, and G_2/M phase) were

495   determined by DNA modeling software (ModFit LT version 4.1). Experiments were repeated a

496   minimum of three times.

497   **Immunofluorescence assays.** Disruptions of microtubule dynamics were distinguishable by using our

498   previously reported immunofluorescence methodology [22]. Briefly, freshly trypsinized cell

499   suspensions (1×10^5-1×10^6) in were seeded in a 12-well plate with glass coverslips. Cells were treated

500   with compounds 1 and 3 for 24 h at various concentrations based on the effective concentrations

501   determined from the cell cycle tests (compound 1 at 25, 250, and 500 nM, and Compound 3 at 25, 250,

502   and 500 nM). Then, the cells were fixed with 4% paraformaldehyde for 1 h and permeabilized with

503   0.2% Tri-tonX-100 (diluted in PBS) for 20 min. The cells were incubated in shakers with the primary

504   antibody against α-tubulin (1:50, diluted in 2% bovine serum albumin) for 1 h at room temperature (or

505   overnight at 4□), followed by Alexa Fluor 488-conjugated Goat Anti-rabbit IgG (H+L) (1:500, diluted

506   in 2% bovine serum albumin) for another hour. Finally, nuclei were labeled with DAPI for 20 min in

507   the dark. Fluorescently labeled cells were imaged using an Olympus BX81 fluorescence microscope

508   system (Olympus, Tokyo, Japan) and a confocal microscope (UltraVIEW$^{®}$VoX).

509   **Surface plasmon resonance-based tubulin binding assays.** The bio-molecular interactions between

510   compounds and tubulin were measured by using surface plasmon resonance (SPR). Epacadostat

511   (INCB024360) was purchased from Cell Signaling Inhibitors Technology (Selleck Chemicals, USA).

512   Briefly, freshly extracted tubulin protein was diluted to 1 mg/mL in PBS (Gibco) and then immobilized

513   in   a   CM5   sensor   chip   by   amine   coupling   NHS/EDC

514   (N-hydroxysuccinimide/N-(3-dimethylaminopropyl)-N'-ethylcarbodiimide   hydrochloride).   The

515   immobilization was up to 800 mDeg (response units). Compounds were diluted two-fold from 80 µM

516   to 2.5 µM in PBS with 0.5% (v/v) DMSO. Compounds (200 µL) at different concentrations were then

517   injected at 60 µL/min for 300 s into PBS containing 0.5% (v/v) DMSO as the running buffer. NaOH

518   (20 mM) was then added for 300 s to dissociate the product. The changes in the SPR were analyzed

519   with Biocore analysis software (BI 2000).

23

Tubulin Assembly. Tubulin (porcine brain, > 99% pure, T240-A) were purchased from the Cytoskeleton company. Both of ligands and work solutions were done in DMSO. A centrifugation of 90000 g was selected for 10 min in a TLA 120 rotor at 4 °C in an Optima TLX centrifuge for removing aggregates. Tubulin was kept at 4 °C, and 0.9 mM GTP and 6 mM $MgCl_2$. The solution was distributed in 200 µL polycarbonate tubes for the TL100 rotor. Growing concentrations of the ligands ranging from 0.05 to 2 µM were added to DMSO content of the samples (1%) with incubation for 30 min at 37 °C. Both supernatants and pellets were diluted 1:5 in the same buffer, and tubulin concentrations were measured fluorometrically (λexc = 280; λems = 323) using tubulin standards calibrated spectrophotometrically. The 50% inhibitory ligand concentration of tubulin assembly was determined with a centrifugation assay.

Evaluation of *in vivo* Antitumor Activity. The animal experiment was carried out in a barrier housing facility by keeping with the national standard of Laboratory Animal-Requirements of Environment and Housing Facilities (GB 14925-2001). The care of laboratory animal and the animal experimental operation conformed to Beijing Administration Rule of Laboratory Animal, *et al*. The investigation conforms the Guide for the Care and Use of Laboratory Animals published by the US National Institutes of Health (NIH Publication No. 85-23, revised 1996). The study protocol was approved by the Laboratory Animal Service Center of Huazhong Agricultural University (Wuhan, China). We promise that the study was performed according to the international, national and institutional rules considering animal experiments, clinical studies and biodiversity rights. Male BALB/c nude mice, 4 weeks old about 15-20 g were purchased and housed at the Laboratory Animal Service Center of Huazhong Agricultural University (Wuhan, China) in pathogen-free conditions, maintained at constant room temperature, and fed a standard rodent chow and water. 1×10^6 cells/mL MCF-7 cells grown in logarithmic phase were resuspended in DMEM medium. 0.1 mL of the cell suspension was injected into the hind legs of each mouse. After implantation, the tumor mass was measured with an electronic

544   caliper twice a week. After the tumor volume reached about 90 mm^3, we placed the xenograft

545   tumor-bearing nude mice into three groups at 5 mice per group: isotonic saline and 0.005% DMSO

546   (control), VP-16, and Compound 3 groups. The reference compound VP-16 and the test Compound **3**

547   were completely dissolved in isotonic saline and 0.005% DMSO due to its relatively lower solubility.

548   The mice were injected at a dose of 20 mg/kg body weight. Tumor volume were recorded every day.

549   **Molecular modeling study.** The crystal structure of tubulin in complex from Protein Data Bank (ID:

550   5JCB) was retrieved as the model structure for assessing the compounds docking with tubulin by using

551   Discovery Studio in School of Pharmaceutical Sciences of Wuhan University. 3D structure of tubulin

552   was prepared by removing podophyllotoxin and water molecule and adding missing hydrogen in the

553   crystal structure. Then applied force field and defined the center of the active site in 1SA1 for ligand as

554   (120, 90, and 7). Compounds were prepared by adding missing hydrogen. And, then the energy

555   minimized atomic coordinates of Compound 3 and 6 were generated using Chemdraw (Chemdraw 3D

556   8.0). The quantum chemically optimized structures of ligands were used as initial structures. The last

557   but one, the advance docking method CDOCKER was used to dock prepared ligand to the colchicine

558   binding site as defined in tubulin for 10 top hits. The minimum free binding energy was selected for

559   further tubulin-ligand interaction analysis.

560   **ACKNOWLEDGMENTS**

565   **References**

566   [1] C. Dumontet, M. Ann Jordan, Microtubule-binding agents: a dynamic field of cancer therapeutics.

567   Nat. Rev. Drug Discov. 9 (2010) 791-803.

568 [2] R. Kaur, G. Kaur, R.K. Gill, R. Soni, J. Bariwal, Recent developments in tubulin polymerization

569   inhibitors: An overview. Eur. J. Med. Chem. 87 (2014) 89-124.

570 [3] A. Massarotti, A. Coluccia, R. Silvestri, G. Sorba, A. Brancale, The tubulin colchicine domain: a

571   molecular modeling perspective. ChemMedChem 7 (2012) 33-42.

572 [4] M.Q. Dong, F. Liu, H.Y. Zhou, S.M. Zhai, B. Yan, Novel natural product- and privileged

573   scaffold-based tubulin inhibitors targeting the colchicine binding site. Molecules 21 (2016) 1375.

574 [5] L. Li, S.B. Jiang, X.X. Li, Y. Liu, J. Su, J.J. Chen, Recent advances in trimethoxyphenyl (TMP)

575   based tubulin inhibitors targeting the colchicine binding site. Eur. J. Med. Chem.151 (2018)

576   482-494.

577 [6] S. Banerjee, K.E. Arnst, Y.X. Wang, G. Kumar, S.S. Deng, L. Yang, G.B. Li, J.L. Yang, S.W.

578   White, W. Li, D.D. Miller, Heterocyclic-fused pyrimidines as novel tubulin polymerization

579   inhibitors targeting the colchicine binding site: structural basis and antitumor efficacy J. Med.

580   Chem. 61 (2018) 1704-1718.

581 [7] X. Yu, Z.P. Che, H. Xu. Recent advances in the chemistry and biology of podophyllotoxins. Chem.

582   Eur. J. 23 (2017) 4467-4526.

583 [8] W. Zhao, C. Zhou, Z.Y. Guan, P. Yin, F.S. Chen, Y.J. Tang, Structural insights into the inhibition

584   of tubulin by the antitumor agent 4β-(1,2,4-triazol-3-ylthio)-4-deoxypodophyllotoxin. ACS Chem.

585   Biol. 12 (2017) 746-752.

586 [9] Y.Q, Liu, J. Tian, K. Qian, X.B. Zhao, S.L. Morris-Natschke, L. Yang, X. Nan, X. Tian, K.H. Lee,

587   Recent progress on C-4-modified podophyllotoxin analogs as potent aantitumor agents. Med. Res.

588   Rev. 35(2015) 1-62.

589 [10] A. Brancale, R. Silvestri, Indole, a CoreNucleus for potent inhibitors of tubulin polymerization.

590   Med. Res. Rev. 27 (2007) 209-238.

591 [11] S.A. Patil, R. Patil, D.D Miller, Indole molecules as inhibitors of tubulin polymerization: potential

592   new anticancer agents, an update (2013-2015). Future Med. Chem. 4 (2012) 2085-2115.

593   [12]G. Hoefle, N. Bedorf, H. Steimetz, D. Schomburg, K. Gerth, H Reichenbach. Epothilone A and

594   B-Novel 16-membered macrolides with cytotoxic activity. Isolation, crystal structure and

595   conformation in solution. Angew. Chem. Int. Ed. Engl. 35 (1996) 1567-1569.

596   [13]A. Coluccia, D. Sabbadin, A Brancale, Molecular modelling studies on arylthioindoles as potent

597   inhibitors of tubulin polymerization. Eur. J. Med. Chem. 46 (2011) 3519-3525

598   [14]H.Y. Lee, J.F. Lee, S. Kumar, Y.W. Wu, W.C. HuangFu, M.J. Lai, Y.H. Li, H.L. Huang, F.C. Kuo,

599   C.J. Hsiao, C.C. Cheng, C.R. Yang, J.P. Liou, 3-Aroylindoles display antitumor activity in vitro

600   and *in vivo:* Effects of N1-substituents on biological activity. Eur. J. Med. Chem. 125 (2017)

601   1268-1278.

602   [15]E. Vitaku, D.T. Smith, J.T.J. Njardarson, J. Med. Chem. Analysis of the structural diversity,

603   substitution patterns, and frequency of nitrogen heterocycles among U.S. FDA approved

604   pharmaceuticals. 57 (2014) 10257-10274.

605   [16]N. Abbassi, E.M. Rakib, H. Chicha, L. Bouissane, A. Hannioui, C. Aiello, R. Gangemi, P.

606   Castagnola, C. Rosano, M. Viale, Synthesis and antitumor activity of some substituted indazole

607   derivatives. Arch. Pharm. Chem. Life Sci. 347 (2014) 1-9.

608   [17]O. Afzal, S. Kumar, M.R. Haider, M.R. Ali, R. Kumar, M. Jaggi, S. Bawa, Europ. A review on

609   anticancer potential of bioactive heterocycle quinoline. Eur. J. Med. Chem. 97 (2015)

610   871-910.

611   [18]W. Zhao, Y. Yang, Y.X. Zhang, C. Zhou, H.M. Li, Y.L.Tang, X.H. Liang, T. Chen, Y.J. Tang,

612   Fluoride-containing podophyllum derivatives exhibit antitumoractivities through enhancing

613   mitochondrial apoptosis pathway by increasing the expression of caspase-9 in HeLa cells. Sci. Rep.

614   5 (2015) 17175.

615   [19]M.M. Magiera, P. Singh, S. Gadadhar, C. Janke, Tubulin posttranslational modifications and

616   emerging links to human disease. Cell 173 (2018) 1323-1327.

617   [20] Y.L. Bennani, W. Gu, A. Canales, F.J. Díaz, B.K. Eustace, R.R. Hoover, J. Jiménez-Barbero, A.

618   Nezami, T. Wang, Tubulin binding, protein-bound conformation in solution, and antimitotic

619   cellular profiling of noscapine and its derivatives. J. Med. Chem. 55 (2012) 1920-1925.

620   [21] W.M. Bonner, C.E. Redon, J.S. Dickey, A.J. Nakamura, O.A. Sedelnikova, S. Solier, Y. Pommier,

621   GammaH2AX and cancer. Nat. Rev. Cancer 8 (2008) 957-968.

622   [22] J.L. Li, W. Zhao, C. Zhou, Y.X. Zhang, H.M. Li, Y.L. Tang, X.H. Liang, T. Chen, Y.J. Tang,

623   Comparison of carbon-sulfur and carbon-amine bond in therapeutic drug: 4β-S-aromatic

624   heterocyclic podophyllum derivatives display antitumor activity. Sci. Rep. 5 (2015) 14814.

625

626 **Table 1.** Virtual screening of podophyllotoxin derivatives by docking with tubulin complexes.

Compound	ΔG (kcal/mol) [a]	Ki (μM) [b]	Hydrogen bonds	π-π bonds
1	-10.85	0.10	α182Val, β124ASP, β241Cys	-
2	-10.26	0.10	α182Val, α178Ser, β124ASP, β241Cys	-
3	-12.88	0.01	α182Val, α178Ser, β241Cys, β124ASP	α241Phe
4	-11.18	0.05	α178Ser, β352Lys, β124ASP, β241Cys	-
5	-10.69	0.02	α182Val, β241Cys, β124ASP	-
6	-12.16	0.06	α182Val, α178Ser, β241Cys, β124ASP	α241Phe
7	-12.34	0.03	α182Val, β238 Val, β241Cys	-
8	-11.46	0.12	α178Ser, α101Asn, β241Cys	-
9	-10.81	0.06	α182Val, α178Ser, β240Thr	α241Phe
10	-10.10	0.11	α178Ser, α111Gln, α180Ala	-
11	-10.64	0.12	α182Val, β238Val, β241Cys	-
12	-10.03	0.19	α178Ser, α101Asn, β238 Val	-
podophyllotoxin	-8.97	0.27	β124ASP, β241Cys	-
Colchicine	-9.57	0.11	β124ASP, β241Cys, β205Gln,	-

627 [a] Estimated free energy of binding (ΔG) in kcal/mol. [b] Estimated inhibition constant (Ki).
628

629 **Table 2.** Anticancer activity and cytotoxicity of podophyllotoxin derivatives.

Compound	Cytotoxic activity (IC$_{50}$, μM) [a]							
	HepG-2	HL-7702	HeLa	H8	A549	MRC-5	MCF-7	HMEC
1	1.8±0.2	33.6±1.5	2.1±0.3	29.2±3.5	2.4±0.2	32.4±2.9	1.3±0.2	64.2±2.4
2	0.9±0.1	43.3±2.8	0.9±0.01	29.2±3.5	0.5±0.01	51.3±3.1	0.4±0.01	55.2±5.3
3	0.1±0.01	94.6±3.2	0.08±0.0	84.5±2.9	0.08±0.0	69.1±2.9	0.07±0.0	61.6±2.3
4	2.5±0.6	30.5±2.7	3.8±0.2	19.4±1.7	2.2±0.9	38.5±0.9	4.8±0.9	45.5±3.5
5	1.2±0.3	41.4±2.2	1.8±0.3	25.6±1.5	2.6±0.3	45.6±2.2	3.0±0.5	60.5±5.6
6	0.3±0.02	50.6±4.9	0.2±0.01	98.4±4.1	0.2±0.01	60.8±4.3	0.2±0.02	81.8±7.2
7	1.9±0.2	38.4±2.6	0.8±0.1	65.5±3.8	1.0±0.1	53.6±0.9	0.8±0.1	52.5±4.4
8	6.3±0.9	29.4±1.7	2.5±0.9	19.5±2.4	5.4±0.2	35.5±1.9	2.7±0.8	43.3±2.6
9	>100	89.8±4.7	>100	94.2±8.2	>100	70.8±6.0	>100	79.8±7.2
10	0.8±0.1	64.3±5.9	0.7±0.1	80.2±6.5	0.3±0.1	22.5±1.8	0.6±0.1	89.2±8.7
11	4.1±1.1	16.3±2.8	3.1±0.2	9.4±1.9	2.3±0.1	25.6±2.9	1.4±0.3	73.5±6.3
12	4.6±0.4	37.0±4.8	2.7±0.3	89.6±3.7	1.2±0.2	49.1±5.3	1.0±0.1	39.2±2.1
Colchicine	5.8±0.1	9.2±0.3	10.2±0.4	6.1±0.4	9.7±0.2	6.2±0.7	14.3±0.5	8.1±0.2
Podophyllotoxin	2.4±0.1	5.0±0.6	6.9±0.1	8.4±0.5	2.6±0.1	10.6±1.2	2.4±0.3	5.6±0.1
Nocodazole	0.4±0.2	13.5±1.5	0.3±0.1	18.0±2.6	0.2±0.05	15.3±1.9	0.2±0.1	11.5±2.2

630 [a] MTT methods, drug exposure was for 48 h, the IC$_{50}$ values was the average of triplicates.

Figure legends

Figure 1. Predicted docking models for podophyllotoxin, 4β-*NH*-(6″-aminoindole)-4-desoxy-podophyllotoxin (Compound **3**) and 4β-*NH*-(5″-aminoindazole)-4-desoxy-podophyllotoxin (Compound **6**) binding in the colchicine-binding site. Tubulin crystal structure, PDB ID: 1SA1.

Figure 2. Predicted docking models for podophyllotoxin, 4β-*NH*-(6″-aminoindole)-4-desoxy-podophyllotoxin (Compound **3**) and 4β-*NH*-(5″-aminoindazole)-4-desoxy-podophyllotoxin (Compound **6**) binding in the colchicine-binding site. Tubulin crystal structure, PDB code: 5JCB.

Figure 3. Structures of podophyllotoxin and related bioactive analogs. Synthesis of new podophyllotoxin derivatives.

Figure 4. Effect of 4β-*NH*-(6″-aminoindole)-4-desoxy-podophyllotoxin (Compound **3**) and 4β-*NH*-(5″-aminoindazole)-4-desoxy-podophyllotoxin (Compound **6**) on cell cycle arrest against MCF-7 (A), A549 (B), and HeLa (C) cell lines. Cell cycle arrest was detected in HeLa cells using propidium iodide (PI) double staining after 24 and 48 h of treatment with VP-16, nocodazole, Compound 3 and 6. Each value represents the mean ± SE of three independent experiments.

Figure 5. Effect of 4β-*NH*-(6″-aminoindole)-4-desoxy-podophyllotoxin (Compound **3**) and 4β-*NH*-(5″-aminoindazole)-4-desoxy-podophyllotoxin (Compound **6**) on cellular apoptosis in MCF-7 (A), A549 (B), and HeLa (C) cell lines. Apoptosis detection in HeLa cells was carried out using annexin V and propidium iodide (PI) double staining after 24 and 48 h of treatment with VP-16,

655 nocodazole, Compound **3** and **6**. Each value represents the mean ± SE of three independent

656 experiments.

657

658 **Figure 6.** Tubulin binding affinities of 4β-*NH*-(6″-aminoindole)-4-desoxy-podophyllotoxin

659 (Compound **3**) and 4β-*NH*-(5″-aminoindazole)-4-desoxy-podophyllotoxin (Compound **6**) by surface

660 plasmon resonance (SPR). The upper panels show raw titration data, and the lower panels are

661 integrated and dilution–corrected peak area plots of the titration data. SPR measurements were used to

662 determine the ligand profile at 25°C.

663

664 **Figure 7.** Inhibition of tubulin assembly in vitro by compounds. Symbols: PTOX (dark square, ■),

665 colchicine (dark diamond, ◆), nocodazole (dark triangle, ▲), Compound 3 (dark circle, ●), and

666 Compound 6 (open circle, ○). Each value represents the mean ± SE of three independent experiments.

667

668 **Figure 8.** 4β-*NH*-(6″-aminoindole)-4-desoxy-podophyllotoxin (Compound **3**) and

669 4β-*NH*-(5″-aminoindazole)-4-desoxy-podophyllotoxin (Compound **6**) disrupted the organization of the

670 cellular microtubule network and induced histone H3 phosphorylation at nanomolar concentrations.

671 The effects of the drug candidates on tubulin polymerization in HeLa cells. Microtubules (green) were

672 stained with α–tubulin antibodies; DNA (blue); and histone phosphorylation (H3) (red). All samples

673 were stained for 24 h.

674

675 **Figure 9.** *In vivo* antitumor activity of 4β-*NH*-(6″-aminoindole)-4-desoxy-podophyllotoxin (Compound

676 **3**) after 3 days, and after administration of Compound 3 at a dose of 40 mg/kg for a week. MCF-7 cell

677 line was used for *in vivo* studies. The images of mice and tumors of each group. Data did not conform

678 to Mauchly's test of sphericity, and a Greenhouse-Geisser correction was performed.

679 **Figure 10.** Structure and electronegativity analysis of podophyllotoxin

680 4β-NH-(6-aminoindole)-4-desoxy-podophyllotoxin or

681 4β-NH-(6-aminoindole)-4-desoxy-podophyllotoxin.

682

683 **Figure 11.** Structure of the tubulin cleavage complex stabilized by podophyllotoxin derivatives.

684 4β-*NH*-(4″-aminoindole)-4-desoxy-podophyllotoxin (Compound **1**)

685 4β-*NH*-(5″-aminoindole)-4-desoxy-podophyllotoxin (Compound **2**)

686 4β-*NH*-(6″-aminoindole)-4-desoxy-podophyllotoxin (Compound **3**) and

687 4β-*NH*-(7″-aminoindole)-4-desoxy-podophyllotoxin (Compound **4**) were found to bind the active site

688 between α /β interfaces with the surface model treatment in 3D image. Active interaction fragments

689 were found to bind the active site between α/β interfaces with the amino acids model treatment.

690 Schematic representation of the interactions between tubulin and Compounds interactions were marked

691 with lines: green dotted lines indicate H-bonds, the orange yellow solid lines were pi-π stacking

692 interactions to the tubulin.

693

694

695

696

697

Figure 1. Zhao, He, Xiang, and Tang
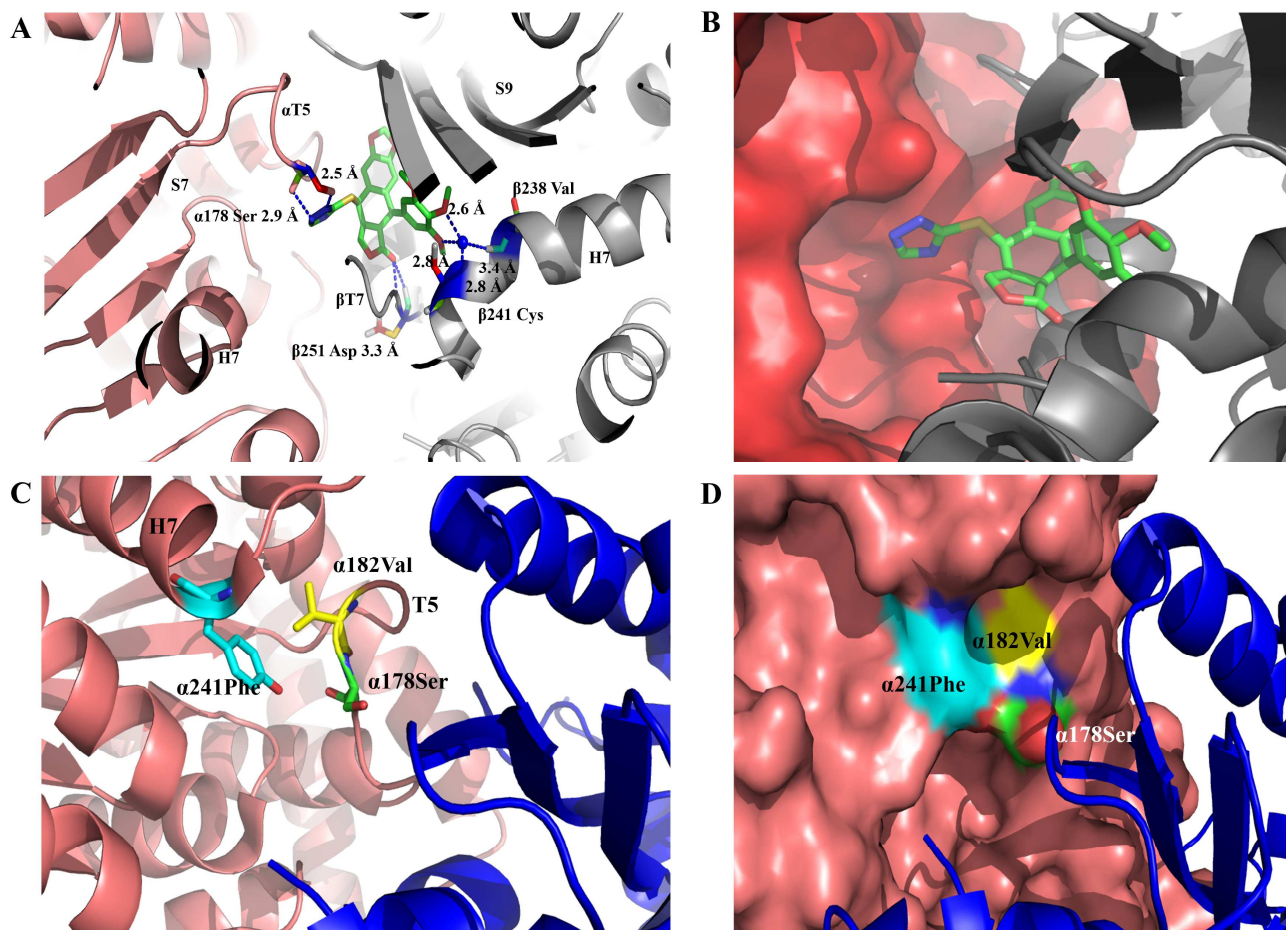
698

699

700

701

702

703

704

705

34

706

707

708

709 **Figure 2. Zhao, He, Xiang, and Tang**

710

Podophyllotoxin → KI/ CH₃CN, 0 °C, 5 min; BF₃OEt₂, rt., 1 h → 4β-iodopodophyllotoxin → THF/BaCO₃, 0 °C, 5 h; TEA, rt., 14 h → Compound 1-12

R (yield)

1 (25%)   2 (33%)   3 (40%)   4 (35%)

5 (32%)   6 (36%)   7 (26%)   8 (30%)

9 (28%)   10 (31%)   11 (37%)   12 (28%)
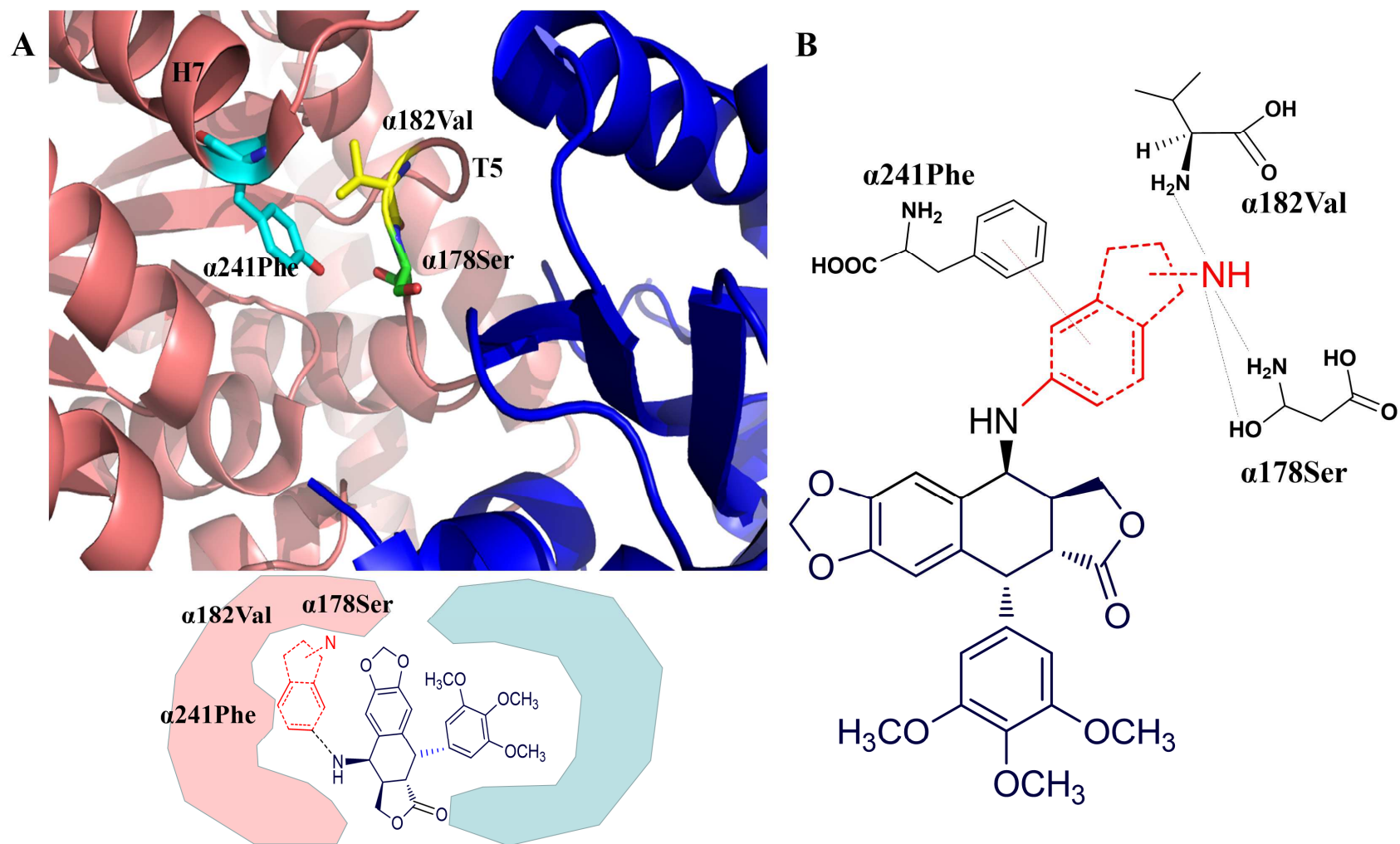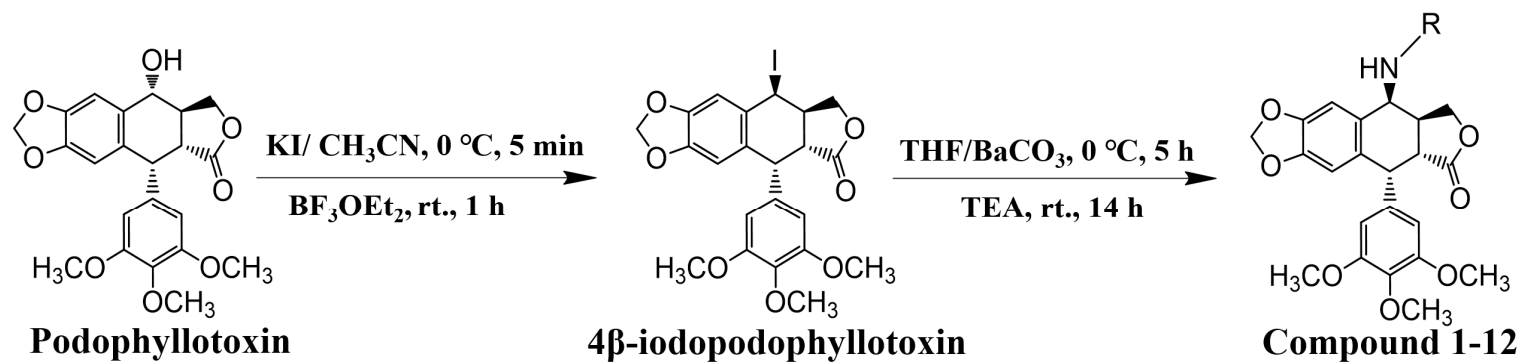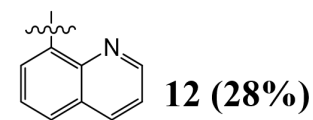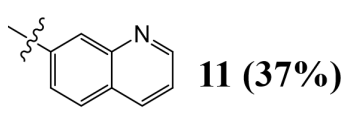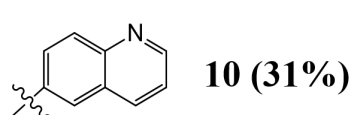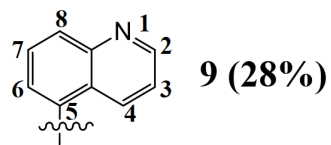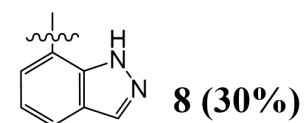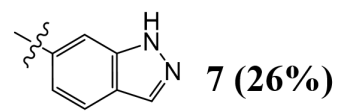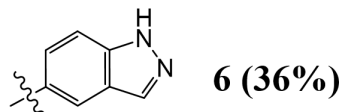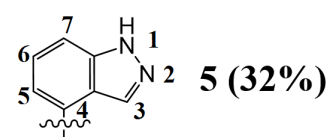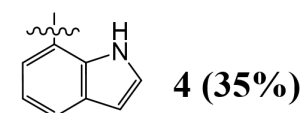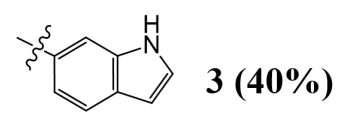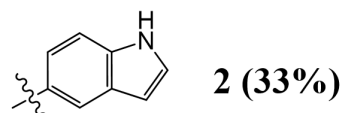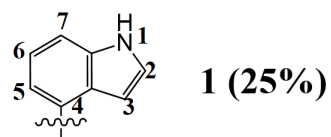
711

712

713

Figure 3. Zhao, He, Xiang, and Tang

714
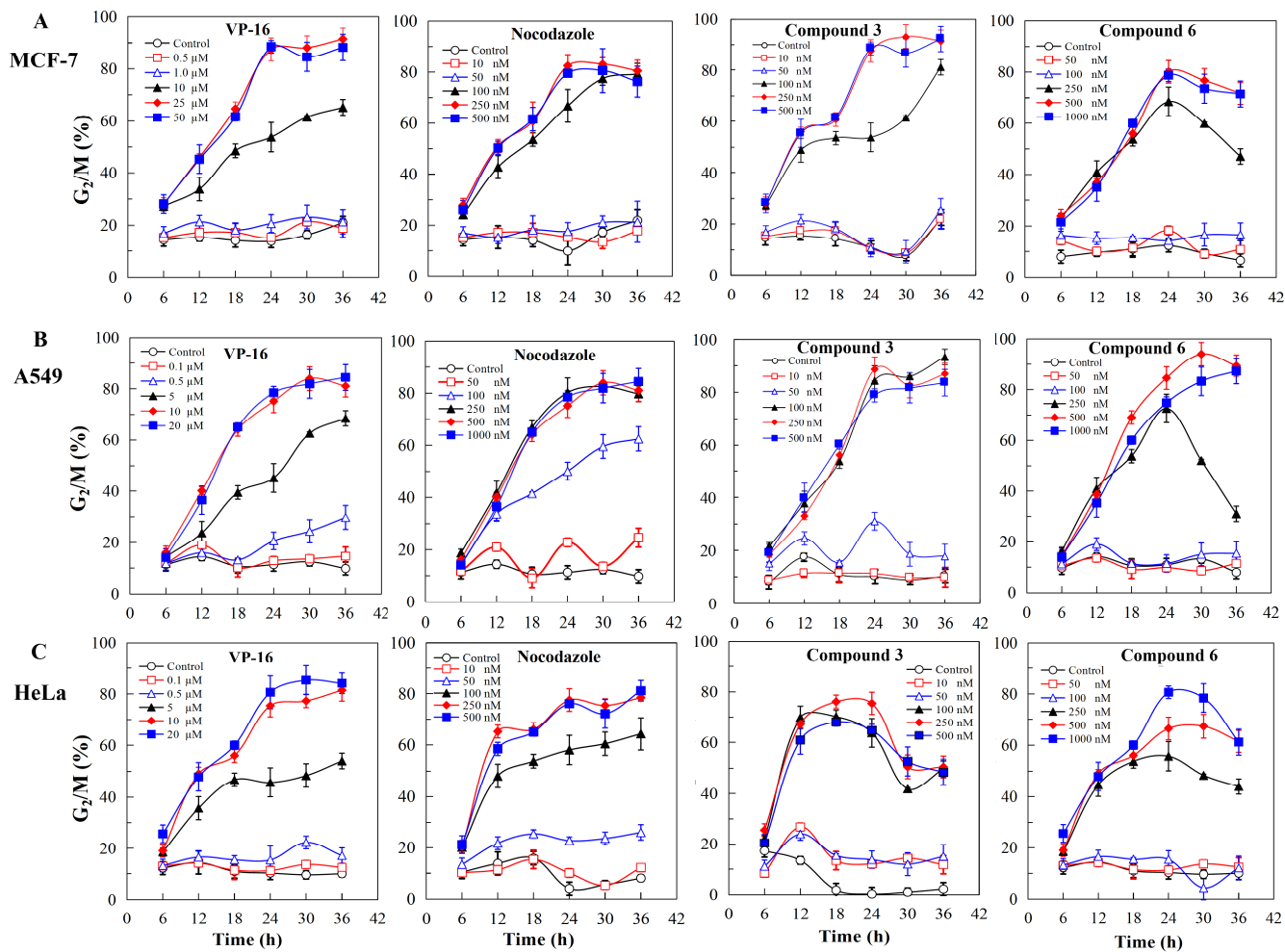
715

716

717

718

719

720 **Figure 4. Zhao, He, Xiang, and Tang**

721

722

723

724

725

726

727
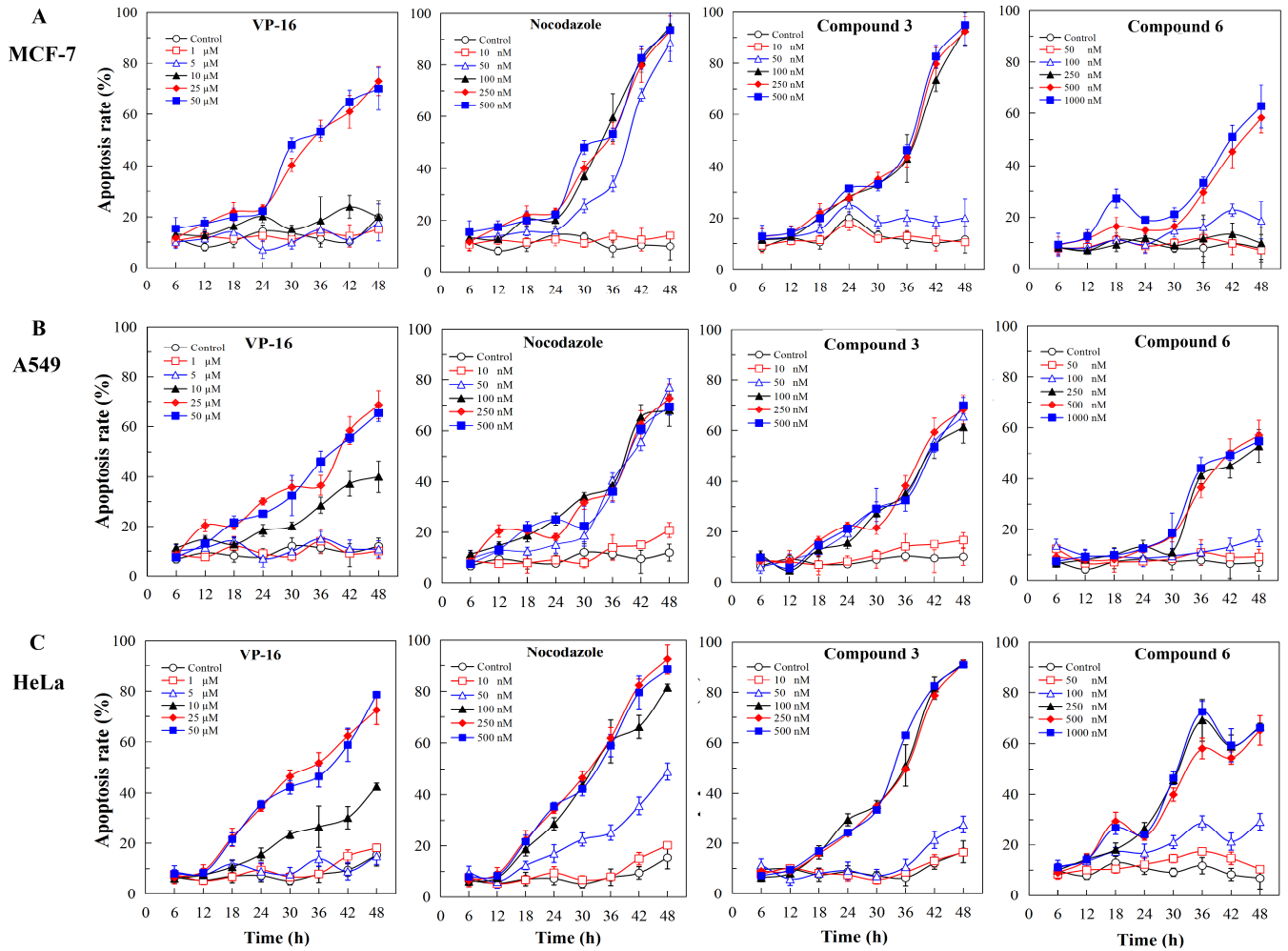
728

729

730

731

732 **Figure 5. Zhao, He, Xiang, and Tang**

38

733

734

735
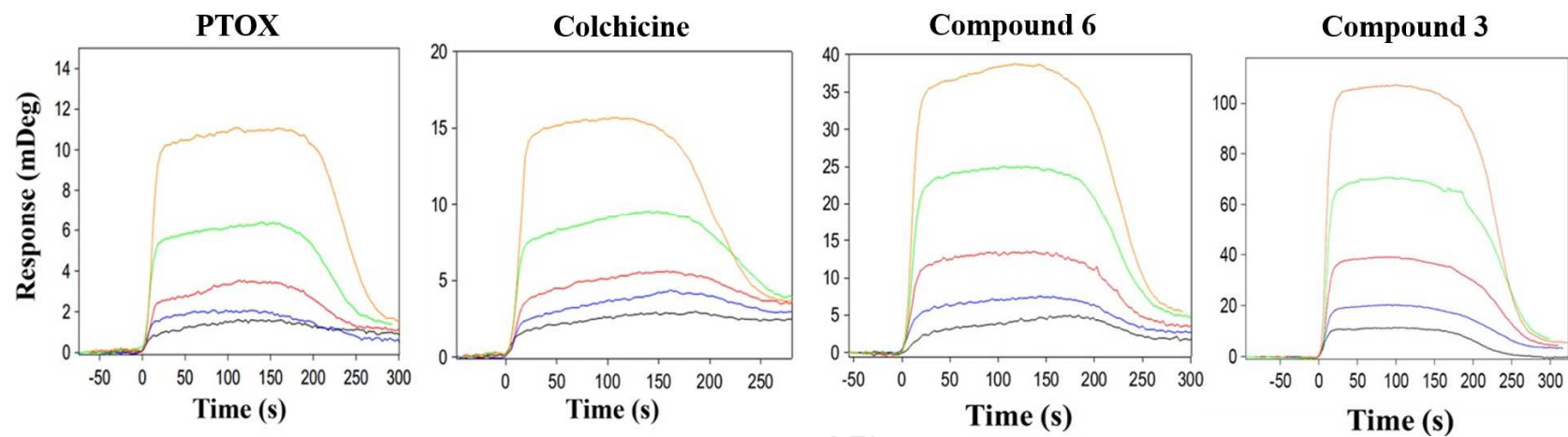
736

737

738

739

740

741 **Figure 6. Zhao, He, Xiang, and Tang**

742
743

744

745

Figure 7. Zhao, He, Xiang, and Tang
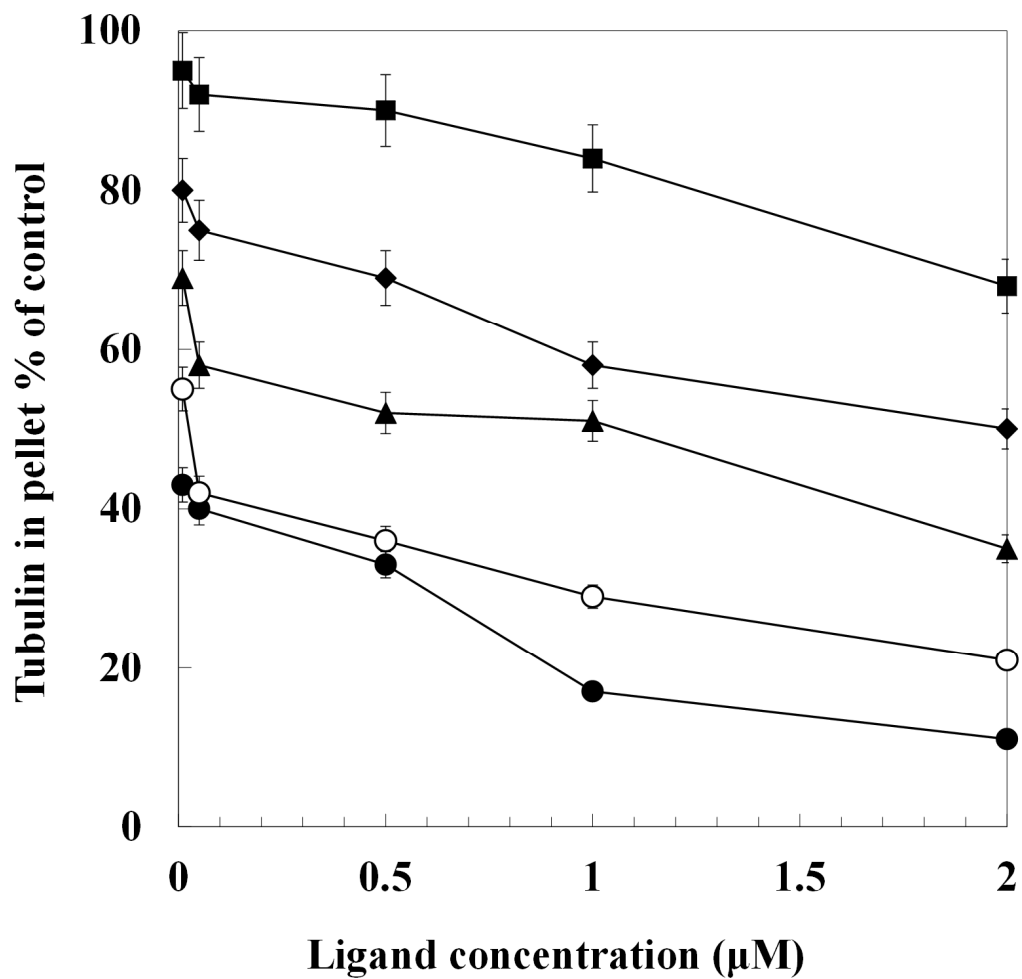
746

747

748

749

750

751
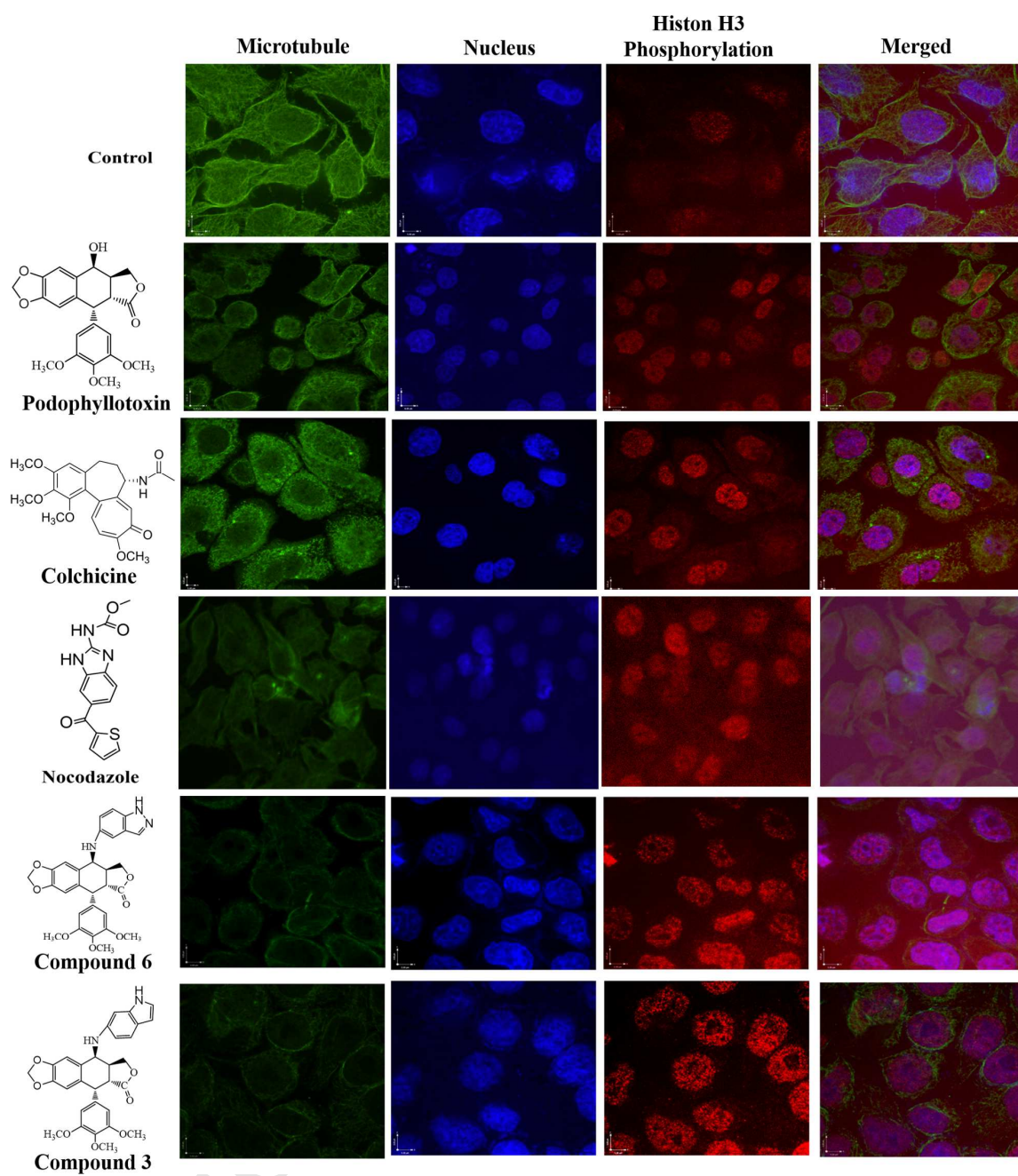
Figure 8. Zhao, He, Xiang, and Tang

758

759

760
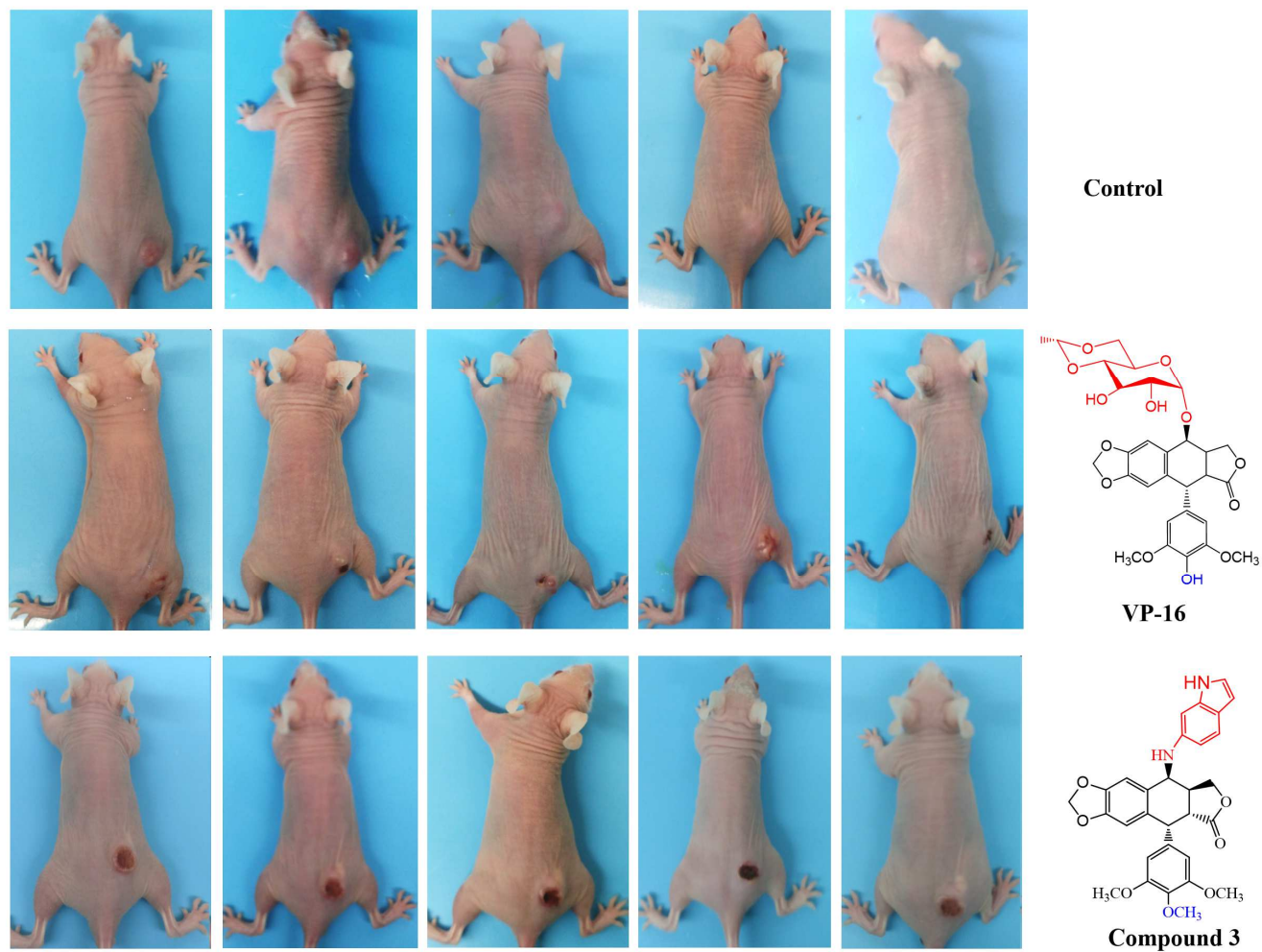
Figure 9. Zhao, He, Xiang, and Tang
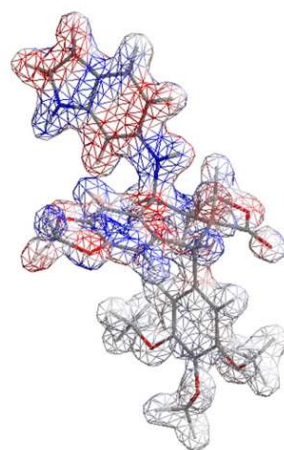
762

42
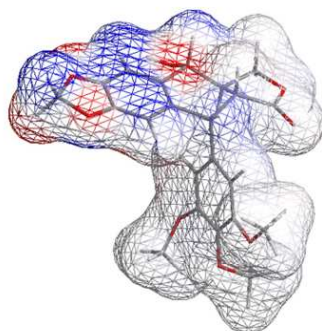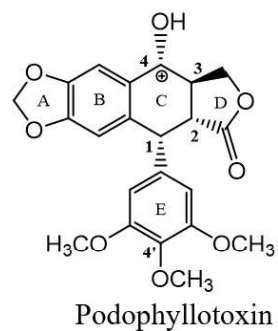
Podophyllotoxin
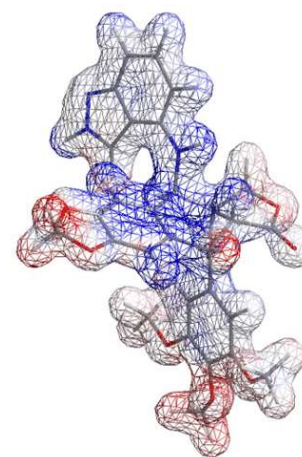
Stretch: 3.1511
Bend: 19.7851
Stretch-Bend: 0.0848
Torsion: -10.1526
Non-1,4 VDW: -7.0950
1,4 VDW: 26.1520
Dipole/Dipole: 5.0243
Total Energy: 38.1052 kcal/mol

Podophyllotoxin

Stretch: 3.7759
Bend: 37.1529
Stretch-Bend: 0.0756
Torsion: -28.2897
Non-1,4 VDW: -4.9291
1,4 VDW: 30.9966
Dipole/Dipole: 6.9635
Total Energy: 45.7457 kcal/mol

4β-NH-(6-aminoindole)-4-
desoxy-podophyllotoxin

Stretch: 3.8602
Bend: 39.0731
Stretch-Bend: 0.0757
Torsion: -22.7120
Non-1,4 VDW: -4.4654
1,4 VDW: 31.4382
Dipole/Dipole: 7.2681
Total Energy: 54.5379 kcal/mol

4β-NH-(6-aminoindole)-4-
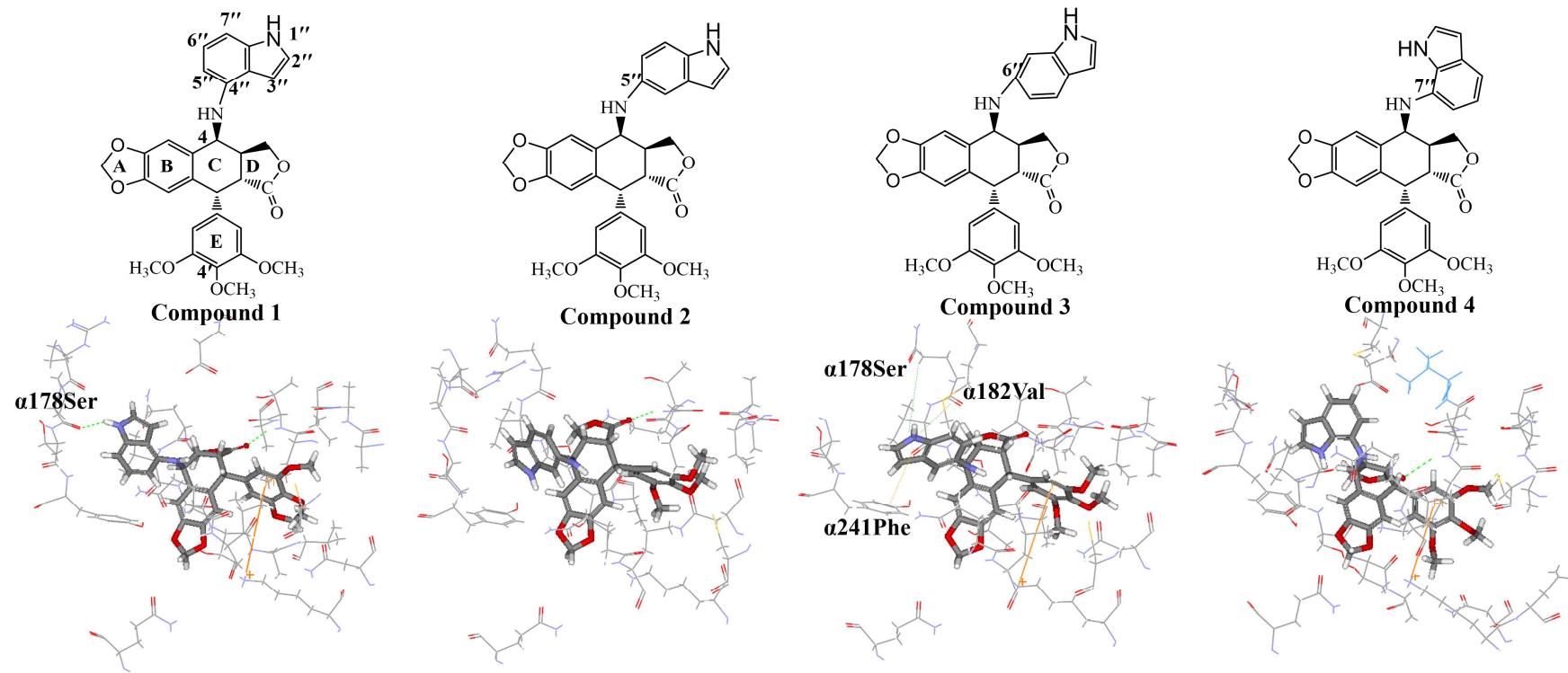desoxy-podophyllotoxin

763

764

765

766

767

768

769 **Figure 10. Zhao, He, Xiang, and Tang**

770

43

771

772

773

Figure 11. Zhao, He, Xiang, and Tang

774

775

776

777

44

Discover 4β-*NH*-(6-aminoindole)-4-desoxy-podophyllotoxin with nanomolar-potency antitumor activity by improving the tubulin binding affinity on the basis of a potential binding site nearby colchicine domain

Wei Zhao [a, 1], Long He [b, 1], Tian-Le Xiang [c] and Ya-Jie Tang [a, b, ∗]

[a] *State Key Laboratory of Microbial Technology, Shandong University, Qingdao 266237, China*

[b] *Hubei Key Laboratory of Industrial Microbiology, Hubei Provincial Cooperative Innovation Center of Industrial Fermentation, Key Laboratory of Fermentation Engineering (Ministry of Education), Hubei University of Technology, Wuhan 430068 China*

[c] *No.11 Middle School of Wuhan, Wuhan 430068 China*

*Corresponding author. Tel. & Fax: +86-27-5975.0491 Email: yajietang@sdu.edu.cn

[1] These authors contributed equally to this work

Highlights

- Drug design on the basis of a potential binding site nearby colchicine domain.

- In theory, Compound **3** formed hydrogen bond to αT5 loop-αH7 and colchicine domain.

- Compound **3** displayed the higher tubulin binding affinity than drug nocodazole.

- Compound **3** exhibited nanomolar-potency antitumor activity on tumor cells.

- Solid tumors were destroyed without lethal toxicity *in vivo* by Compound **3**.